Journal of Advanced Research 79 (2026) 783–799

Contents lists available at ScienceDirect

Journal of Advanced Research

journal homepage: www.elsevier.com/locate/jare

Inflammation-driven biomimetic nano-polyphenol drug delivery system alleviates severe acute pancreatitis by inhibiting macrophage PANoptosis and pancreatic enzymes oversecretion

Junyong Wu [a,b], Hai Huang [a,b], Wenjie Xu [a,b], Beibei Cui [c], Pengcheng Sun [a,b], XinYan Hao [a,b], Shihe Jiang [c], Xuyang Hou [c], Xiaoyan Qi [c], Zuxing Wei [c], Yimiao Cheng [c], Yanwen Zheng [c], Kuijie Liu [c,*], Jun He [c,*]

[a] Department of Pharmacy, The Second Xiangya Hospital Central South University Changsha 410011, China
[b] Institute of Clinical Pharmacy Central South University Changsha 410011, China
[c] Department of General Surgery, The Second Xiangya Hospital, Central South University, Changsha, Hunan 410011, China

HIGHLIGHTS

- We developed a biomimetic self-assembly nanoparticle (FePTX@CM NPs) alleviate macrophage PANoptosis and enzyme oversecretion in SAP.
- PYD in the NPs inhibited pancreatic enzyme release by mitochondrial ROS/Golgi stress, while PTX prevented macrophage PANoptosis by Zbp1 inhibition.
- FePTX@CM NPs exhibited pancreas targeting ability due to the inflammation-driven macrophage membrane on its surface.

GRAPHICAL ABSTRACT

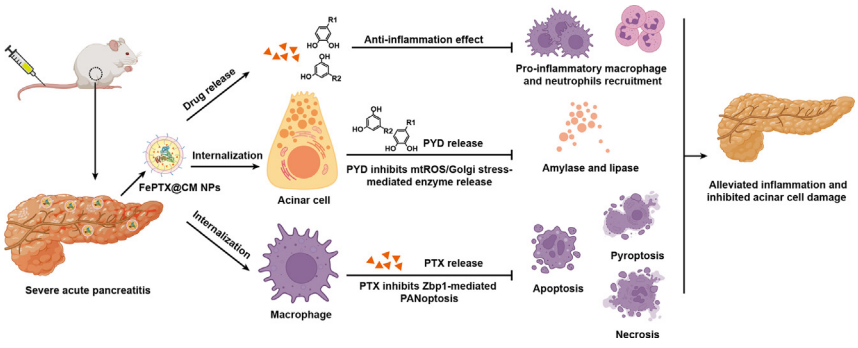

ARTICLE INFO

Article history:
Received 11 October 2024
Revised 22 March 2025
Accepted 2 April 2025
Available online 8 April 2025

Keywords:
Severe acute pancreatitis
PANoptosis
Inflammation-driven
Biomimetic nanoparticle
Enzyme secretion

ABSTRACT

Introduction: Severe acute pancreatitis (SAP) is a critical inflammatory disease with high morbidity and mortality. Current treatments focused on symptomatic relief but failed to prevent inflammation progression in cellular level.

Objectives: In order to develop an SAP-targeting drug delivery system to alleviate SAP in cellular level and illustrate its mechanism, we explored the use of proanthocyanidin (PYD) and pentoxifylline (PTX) loaded into macrophage membrane-coated self-assembly nanoparticles (FePTX@CM NPs) for targeted SAP treatment. The combination application of these two drugs was innovative in SAP aid.

Methods: We developed the NPs by self-assembly strategy and cell membrane coating. Its particle size and zeta potential were measured by dynamic light scatter (DLS). The morphology of the NPs was observed by transmission electron microscopy (TEM). And the encapsulation efficiency was evaluated by nano-flow cytometry. The total protein profile was determined via Coomassie brilliant blue. We explore the mechanism of our NPs against SAP in cellular and animal levels. Bioinformatics approaches, TEM, immunofluorescent assay and co-immunoprecipitation were performed to comprehensively explain the specific anti-SAP mechanism of FePTX@CM NPs.

Abbreviations: AP, acute pancreatitis; BSA, biomacromolecules; BFA, Brefeldin A; BMDM, bone marrow-derived macrophage; CM, cell membrane; DLS, dynamic light scatter; Dex, dexamethasone; mtROS, mitochondrial reactive oxygen species; MPS, mononuclear phagocyte system; MODS, multiple organ dysfunction syndrome; NPs, nanoparticles; PYD, proanthocyanidin; PTX, pentoxifylline; SAP, severe acute pancreatitis; SIRS, systemic inflammatory response syndrome; TEM, transmission electron microscopy; TAC, taurocholic acid sodium.

* Corresponding authors.
E-mail addresses: liukuijie@csu.edu.cn (K. Liu), 508104@csu.edu.cn (J. He).

https://doi.org/10.1016/j.jare.2025.04.006

Results: After inflammation-driven targeting, PYD in the NPs inhibited pancreatic amylase and lipase release by suppressing mitochondrial reactive oxygen species (mtROS)/Golgi stress, while PTX prevented SAP-associated macrophage PANoptosis by inhibiting Zbp1 signal pathway. The protection effect of these biomimetic NPs worked from different aspects to alleviate SAP symptoms and inflammation progression in relative cells.

Conclusion: The FePTX@CM NPs demonstrated effective pancreas targeting, reduced systemic inflammation especially pro-inflammatory cell recruitment and activation, and minimized tissue damage in SAP mouse models, offering a promising therapeutic strategy for clinical SAP management.

Introduction

Acute pancreatitis (AP) is an acute inflammatory disease caused by abnormal activation of digestive enzymes within the pancreas. Its characteristics include self-digestion, inflammation, bleeding, and necrosis of pancreatic tissue [1]. Severe acute pancreatitis (SAP) is a severe manifestation of AP and is characterized by high morbidity and mortality [2–4]. Despite an overall decrease in mortality in the last decade, SAP remains a devastating disease with mortality rates ranging from less than 10 % to as high as 30 %. Common triggers include cholelithiasis, alcohol abuse, overeating, drug reactions, and hyperlipidemia [5] Fig. 1.

In the pathological mechanism of acute pancreatitis, inflammatory cells such as macrophages and neutrophils migrated to the damaged site and activated, releasing various pro-inflammatory mediators like IL-6, IL-1β, reactive oxygen species (ROS) leading to a cascade inflammatory response, pancreatic tissue damage and even systemic inflammatory response syndrome (SIRS) and multiple organ dysfunction syndrome (MODS) [6,7]. Therefore, in response to the current symptoms of SAP, clinical treatment mainly focuses on symptomatic therapy including fasting, intravenous fluid therapy, anti-microbial therapy, anti-inflammation therapy and usage of painkillers, etc. [8–10]. However, though supportive therapy can alleviate symptoms to a certain extent, it cannot fundamentally prevent the progression of inflammation or mitigate damaged tissues. Also, the side effects of antibiotics, persistent intravenous transfusion and invasiveness of surgical treatment remain challenges. Therefore, there is an urgent need to develop novel drug formulations aiming at alleviating tissue damage and systemic inflammation at the cellular level.

In recent decades, reports have discovered that polyphenols exhibited multiple anti-inflammatory, antioxidant and antibacterial capabilities in various diseases [11,12]. Polyphenols have been applied in pancreatitis and its complications to alleviate the overactivated inflammation response [13,14]. Proanthocyanidin (PYD) is natural polyphenolic compounds widely found in plants and is now internationally recognized as effective natural antioxidants for scavenging free radicals in many biomedical applications such as cardiovascular health protection, anti-hypertension, anti-tumor and skin cosmetology [15]. In our preliminary research, PYD was confirmed to inhibit amylase and lipase release in pancreatic acinar cells which was of great significance in pancreas protection. This interesting discovery encourages us to further develop PYD for clinic translation. Nevertheless, PYD lacks the ability to positively target pancreas and is often eliminated by mononuclear phagocyte system (MPS) engulfment. Accordingly, developing a proper nano-system to deliver PYD into pancreas is a promising strategy to enhance its clinical values. Considering its chemical structure of polyphenol, PYD was able to coordinate with metal ions such as iron ion (Ⅲ) to form nanoparticles (NPs) as reported previously [16–18]. Though polyphenols were proven to have high affinity with mitochondrial outer membrane proteins [19], it still needed a better targeting strategy to further enhance the accumulation of NPs in pancreas. Biomimetic modification of NPs has emerged as a novel promising strategy to improve targeting ability in drug delivery [20]. Nowadays, various biomimetic approaches have been developed, including peptide insertion [21], membrane fusion [22] and cell membrane coating [23,24], etc. To avoid MPS engulfment, using homologous cell membrane coating may be a better pathway to enable NPs to achieve pancreatic tissues. Meanwhile, macrophages that are recruited to pancreas also influence the whole inflammation progression. Thus, coating macrophage membranes onto the surface of NPs may bring exciting pancreas-targeting effects and surprising efficacy associated with macrophages in SAP microenvironment.

Given the circumstances that the single therapeutic effect induced by PYD may not be sufficient to relieve excessive stress in SAP, we found another classic drug to further function synergistically. Pentoxifylline (PTX) is a xanthine derivative and conventionally used to treat muscle pain in patients with peripheral artery disease [25]. However, it has been reported to regulate immune response and attenuate pulmonary inflammation by inhibiting neutrophils activation [26]. Thus, PTX provided a protective option for SAP treatment. We then discovered the macrophage-protective effect of PTX in SAP progression in a previous study. During SAP, macrophages were recruited into inflammatory pancreas by various mediators, and overactivated macrophage may lyse and release many more factors and toxic substances to enhance excessive inflammation [27]. Importantly, we confirmed that PTX could help macrophages escape from pyroptosis, apoptosis and necrosis (known as PANoptosis), a newly established process essential for stimulating the pro-inflammatory response induced by damage-associated molecular patterns (DAMPs) [28]. This discovery holds significant value in alleviating the overactivated immunity during SAP.

Here, we used nanotechnology to prepare a biomimetic nanoparticle loaded with these two drugs. Fe^{3+} coordinated with polyphenol PYD to form the FePYD NPs, and PTX was added into the NPs for drug loading (FePTX NPs). Then the surface of FePTX NPs was coated with macrophage cell membrane to prepare FePTX@CM NPs. The NPs exhibited good pancreas targeting and biocompatibility in SAP. We verified the efficacy of FePTX@CM NPs in two SAP mice models. We discovered that PYD inside the NPs exhibited an enzyme release suppression effect and acinar cell protection property by alleviating the mitochondrial ROS (mtROS) mediated Golgi stress. Meanwhile, PTX inhibited macrophage PANoptosis, remarkably alleviated the excessive immune stress in pancreatic tissues through the Zbp1 signaling pathway. The synergistic effect presented as reduced systemic inflammation and pancreas with less damage. Therefore, the FePTX@CM NPs bring an exciting insight to reduce tissue damage and develop novel biomimetic drug delivery systems for SAP treatment at the cellular level, offering a valuable reference to clinical practice.

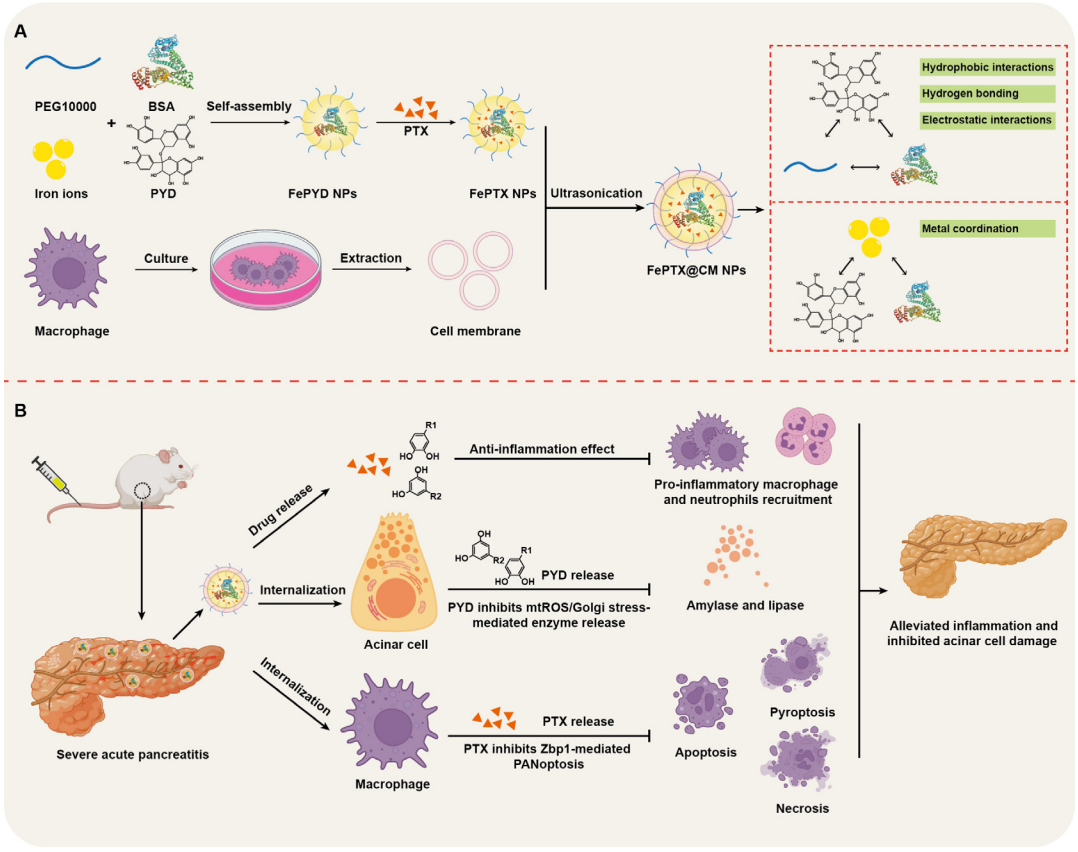

Fig. 1. Schematic illustration of FePTX@CM NPs against SAP. (A) The preparation of FePTX@CM NPs. (B) Mechanisms of FePTX@CM NPs in SAP treatment. After intravenous injection, FePTX@CM NPs targeted the damaged pancreas. On the one hand, drugs released from NPs could suppress the pro-inflammatory mediators release and the recruitment of macrophages and neutrophils to limit systemic inflammation. On the other hand, SAP-associated macrophages and acinar cells internalized NPs and then drugs were released in the cytoplasm. PTX prevented macrophage PANoptosis by inhibiting the Zbp1 signal pathway. And PYD inhibited mtROS/Golgi stress to limit amylase and lipase release.

Materials and methods

Materials

PEG10000 (cat. A601789), $FeCl_3{\cdot}6H_2O$ (cat. A600454) and bovine serum albumin (BSA, cat. A602440) were obtained from Sangon Biotech (Shanghai, China). Proanthocyanidin (PYD, cat. R097064) was obtained from Rhawn Chemistry (Shanghai, China). Pentoxifylline (PTX, cat. HY-B0715) was purchased from MedChemExpress LLC (USA). Dulbecco's modified Eagle's minimum essential medium (DMEM) and fetal bovine serum (FBS) were purchased from Biological Industries (Israel). Cell Counting Kit-8 (CCK8) was purchased from NCM Biotech (Suzhou, China). DiR and DiL dye were purchased from Yeasen Biotechnology (Shanghai, China). All cell culture plates, dishes, transwell plates, ultrafiltration tubes and centrifuge tubes were purchased from NEST Biotechnology (Wuxi, China). MitoSOX red and MitoSOX green were acquired from Sigma-Aldrich (cat. M36008, cat. M36006, Germany). Taurocholic acid (TAC, cat. 86339) was purchased from Sigma-Aldrich (Germany). Caerulein (cat. S9690), Rotenone (cat. S2348) and Brefeldin A (BFA, cat. S7046) were purchased from Selleck Chemicals LLC (Japan).

Cell culture and Animals

AR42J cell line, 266-6 cell line and RAW264.7 cell lines were obtained from National Collection of Authenticated Cell Cultures and maintained in DMEM medium containing $NaHCO_3$ 1.5 g/L, glucose 2.5 g/L and Sodium Pyruvate 0.11 g/L and supplemented with 10 % FBS and 1 % antibiotics (penicillin and streptomycin). Cells were incubated at 37 ℃ in humidified air with 5 % CO_2. Male C57BL/6J (6–8 weeks old) were obtained from SJA Laboratory Animal Co, LTD (Changsha, China) and housed following the guidelines of the Institutional Animal Care and Use Committee (IACUC).

The preparation and characterization of FePYD@CM NPs and FePTX@CM NPs

Preparation of both NPs

The solution of PEG10000 (20 mg/ml), PYD (5 mg/ml), $FeCl_3{\cdot}6H_2O$ (5 mg/ml) and BSA (10 mg/ml) were dissolved by distilled water. 2 ml of water was added into a glass bottle, then 200 μl PEG10000, 100 μl BSA, 200 μl PYD, 200 μl $FeCl_3{\cdot}6H_2O$ were also added into the system in turn. The whole mixture was stirred under room temperature with 1000 rpm for 20 min to prepare FePYD NPs. Then the cell membrane from macrophage (2 mg/ml) was added into the FePYD NPs solution (the volume ratio of FePYD and CM was 1:1) under ultrasonication for 2 min. Then the FePYD@CM NPs were prepared. Then the NPs solution was centrifuged under 13,000 rpm for 10 min and collected pellet for later use. For the preparation of FePTX@CM, 200 μl Pentoxifylline (PTX, 5 mg/ml) was added in the primary solution for drug loading.

Characterization of both NPs

The size and zeta potential of nanoparticles were analyzed by dynamic light scatter (DLS). Transmission electron microscope

(TEM) was used to observe the morphology. Coomassie blue staining was performed to further investigate whether CM was coated onto the NP surface. The drug release profile was measured by the ultrafiltration method. Elemental mapping analysis was used to observe the elemental composition and distribution of the NPs. To investigate the encapsulation efficiency of CM on NPs, DiL was used to label CM. After centrifugation, free DiL was removed. Then Dil-FePYD@CM NPs were prepared. Nano-flow cytometry was performed to detect the fluorescence on NPs. To investigate the main interaction forces of assembly NPs, we added NaCl, Urea, SDS to the NPs solution and determined particle size to observe changes.

Cellular uptake assessment of FePYD@CM

RAW264.7 and 266-6 cells were seeded in a 24-well plate at a density of 1×10^5 cells per well and incubated overnight to facilitate cell attachment. Subsequently, the culture medium was removed and replaced with a fresh medium containing free DiL, DiL-FePYD, DiL-FePYD@CM (the concentration of DiL was 10 μg/mL) for 4 h at 37 °C in an incubator. Post-incubation, the cells were washed three times with phosphate-buffered saline (PBS) to remove any non-internalized particles. The cells were subsequently fixed with 4 % paraformaldehyde for 15 min at room temperature in a dark environment to preserve cellular structures. After fixation, the cells were washed three times with PBS under gentle shaking conditions. To stain the cell nuclei, DAPI was applied for 15 min in a dark environment, followed by three additional PBS washes. Finally, the stained cells were observed by confocal laser scanning microscope (ECHO Revolve Microscope, USA). The cellular uptake of FePYD@CM was also quantified by flow cytometry.

Evaluation of pancreas targeting ability of FePTX@CM NPs

C57BL/6J mice were purchased from SJA Laboratory Animal Co, LTD (Changsha, China). Mice were maintained under pathogen-free conditions. The project was approved by the Second Xiangya Hospital of Central South University Ethics Committee and abide by the animal care and use guidelines. Six to eight weeks old C57BL/6J male mice were fasted for 12 h and randomly divided into 3 groups: free DiR, DiR-labeled FePYD and DiR-labeled FePYD@CM. Then mice were intraperitoneally injected with caerulein (cat. S9690, Selleck, Japan) (50 μg/kg) every 1 h (12 times). After the 6th injection, mice were injected intravenously in three different formulations. When completing all administration (8 h after drug injection), mice were monitored under the In Vivo Imaging System (IVIS) to observe fluorescent intensity. Excised pancreas and other organs (including heart, liver, spleen, lung, kidney, gut) were also imaged via IVIS to determine the biodistribution of FePYD@CM NPs throughout the body.

Biosafety investigation of FePTX@CM NPs

The biosafety assessment assay of FePTX@CM NPs was conducted in healthy mice. The mice were randomly divided into six groups: PBS, PYD, PTX, PYD + PTX, FePTX, FePTX@CM NPs (n = 3). The dosage of PYD was 5 mg/kg and PTX was 1 mg/kg. All formulations were administered intravenously for five times with an interval of two days. After the end of administration, mice were executed, and blood samples were obtained to measure the serum level of ALT, AST, BUN and Cr for the evaluation of function of liver and kidney. All major organs including heart, liver, spleen, lung and kidney were collected for later H&E staining to observe organic damage.

Isolation of bone marrow-derived macrophages and pancreatic acinar cells

C57BL/6J mice were euthanized via CO_2 asphyxiation. The femur and tibia were isolated and extracted under aseptic conditions and then immersed in sterile PBS. The knee joints were removed, exposing the bone marrow cavities at both ends, which were flushed out using a sterile syringe. The cells were expelled and passed through a 40 μm cell filter. The solution was centrifuged at 800 rpm for 5 min to discard the supernatant. The cellular pellet was resuspended in sterile PBS, centrifuged again, and this process was repeated twice. Finally, the cells were resuspended in complete DMEM containing 10 % FBS, 1 % penicillin/streptomycin, and 20 ng/ml M–CSF (cat. 315-02, Proteintech, USA). The cells were counted and inoculated onto cell culture plates, then placed in an incubator with 5 % CO2 at 37 °C. After 24 h, the medium was changed to remove unattached cells. The cells typically differentiate into mature macrophages within approximately 7 days of culture.

RNA-sequencing

RNA sequencing (RNA-seq) was conducted by Novogene in China, following these general steps: First, total RNA was extracted from BMDM cells after the specified treatments, which included 5 μg/ml PTX + 100 ng/ml LPS, FePTX (equivalent concentration of 5 μg/ml PTX) + 100 ng/ml LPS, FePTX@CM (equivalent concentration of 5 μg/ml PTX) + 100 ng/ml LPS, and 100 ng/ml LPS as well as a negative control. The concentration and purity of each RNA sample were assessed using an Agilent 2100 Bioanalyzer. Approximately 1 μg of total RNA from each sample was then used to generate cDNA fragments preferentially sized between 370–420 bp. The library fragments were purified with the AMPure XP system (Beckman Coulter, Beverly, USA). Library construction was completed via PCR using Phusion High-Fidelity DNA Polymerase, universal PCR primers, and Index (X) Primer. Clustering was performed on the Illumina NovaSeq platform to sequence the library and obtain 150 bp paired-end reads. Finally, data analysis was carried out, encompassing quality control, read mapping to the reference genome, quantification of gene expression levels, differential expression analysis, differential expression gene enrichment analysis, and gene set enrichment analysis.

RNA extraction and qRT-PCR

The target tissues or cells were collected and washed with cold PBS. Trizol reagent (cat. 9109, Takara, Japan) and trichloromethane (cat. 10006862, GuoYao Corp, China) were then added in a 5:1 ratio, vortexed, and mixed thoroughly. The mixture was allowed to stand at room temperature for 5 min, followed by centrifugation at 4 °C for 15 min at 12,000 g. The supernatant was collected, and an equal volume of isopropanol (cat. 40064360, GuoYao Corp, China) was added. This solution was mixed by inversion several times and subsequently centrifuged at 4 °C for 10 min at 12,000 g. The supernatant was discarded to yield a white precipitate.

Next, an appropriate volume of 75 % ethanol (cat. 801769610, GuoYao Corp, China) was added, and the mixture was centrifuged at 4 °C for 5 min at 8,000 g. The supernatant was discarded, and Diethylpyrocarbonate (DEPC) water (cat. R0021, Beyotime, China) was added to dissolve the precipitate, resulting in RNA. The purity and concentration of the RNA samples were measured using a Nanodrop 2000 spectrophotometer (Thermo Fisher, USA).

Subsequently, the RNA was reverse transcribed into cDNA using a high-capacity cDNA reverse transcription kit (K1622, Thermo Fisher, USA). The required primers were designed with the following sequences:

IL-1β: TGGACCTTCCAGGATGAGGACA (Forward), GTTCATCTCGGAGCCTGTAGTG (Reverse).

IL-6: TACCACTTCACAAGTCGGAGGC (Forward), CTGCAAGTGCATCATCGTTGTTC (Reverse).

Amylase: CAGCACTTGTGGCAATGACTGG (Forward), GCAAAAGGCTGACCATTGACGAC (Reverse).

Lipase: CCCCCAGATGGGTCATTACG (Forward), CAACGTGCGAAGTTGCTCTT (Reverse).

Zbp1: GATCTACCACTCACGTCAGGAAG (Forward), GGCAATGGAGATGTGGCTGTTG (Reverse).

Actb: CATTGCTGACAGGATGCAGAAGG (Forward), TGCTGGAAGGTGGACAGTGAGG (Reverse).

16srRNA: TCGTCGGCAGCGTCAGATGTGTATAAGAGACAGCCTACGGGNGGCWGCAG (Forward), GTCTCGTGGGCTCGGAGATGTGTATAAGAGACAGGACTACHVGGGTATCTAATCC (Reverse).

The reaction system was prepared using 2X Universal SYBR Green Fast qPCR mix (RK21203, Abclonal, China) kit, and the reaction was carried out on a PCR instrument Light Cycler 96 system (Roche, USA), and the data were finally analyzed.

Protein isolation and western blot assay

Protein isolation

Target tissues or cells were collected and washed with cold PBS. Appropriate amounts of protein lysate containing protease inhibitors (cat. 04693159001, Roche, USA), phosphatase inhibitors (cat. 04906837001, Roche, USA), and RIPA buffer (cat. 89901, Thermo Fisher, USA) were added, and the mixture was sonicated using an ultrasonic splicer for several seconds. The samples were then incubated on ice for 30 min and centrifuged at 12,000 g for 15 min at 4 °C to collect the supernatant containing the proteins.

Western blot assay

The protein concentration was determined using a BCA protein quantification kit (cat. 23225, Thermo Fisher, USA) by measuring the absorbance value at 562 nm with a microplate reader. Based on the protein concentration, the appropriate volume of loading buffer (cat. R095296, RHAWN, China) was added to prepare the protein samples. The samples were denatured by incubating in a metal bath at 100 °C for 10 min.

Modified protein samples were then loaded into the lanes of an electrophoresis tank, where they were subjected to constant voltage electrophoresis at 60 V for 35 min, followed by 120 V for 60 min. Subsequently, the proteins were transferred to a methanol-activated PVDF membrane at a constant voltage of 66 V for 3 h. The samples were then incubated in 5 % milk for 1.5 h at room temperature. Antibodies included anti-cleaved casp1 (cat. 89332S, CST, USA), cleaved-caspase 3 (cat. 9661, CST, USA), caspase 9 (cat. A0281, Abclonal, China), cleaved caspase 9 (9505S, CST, China), β-actin (cat. AC038, Abclonal, China), p-MLKL (cat. AF7420, Affinity, China, China), MLKL (cat. A17312, Abclonal, China), p-RIPK3 (cat. 91702S, CST, USA), RIPK3 (10188S, CST), cleaved casp9 (cat. 9509, CST, USA), ZBP1 (sc-271483, Santa, USA), Amylase (sc-46657, Santa, USA), Lipase (cat. 11209-1-AP, Proteintech, USA) and casp6 (cat. ab185645, Abcam, USA) were incubated overnight on a shaker at 4 °C. The following day, the primary antibody was removed by washing with TBST solution, and the secondary antibody was incubated for 1 h at room temperature. Finally, immune complexes were detected using enhanced chemiluminescence (Life Tec, USA). The bands were quantified with ImageJ software.

PI staining

The BMDM cells were cultured, seeded, and treated according to the specified conditions (see experimental results for details). The medium was discarded, and the cells were washed twice with PBS. Next, 500 μL of 1x PI dye (cat. ST512, Beyotime, China) was added to each group of cells, which were then incubated at 37 °C in the dark for 20 min before being washed twice with PBS. The cells were subsequently mounted on slides and observed under a microscope (ZEN, Germany) for imaging and analysis.

Electron microscope

The BMDM cells were washed three times with PBS. An appropriate volume of trypsin (cat. C3530-0500, VivaCell, USA) was added. The cells were then placed in a cell incubator at 37 °C for 5 min. When most of the cells exhibited a rounded shape, indicating sufficient digestion, the process was halted by adding complete medium. The cells were gently resuspended to detach them from the culture dish, resulting in a single-cell suspension.

This single-cell suspension was transferred to a 1.5 mL Eppendorf tube and centrifuged at 1000 rpm/min for 5 min at room temperature. The supernatant was discarded to obtain the cell pellet. Next, 1 mL of electron microscope fixative (cat. G1102, Serbicebio, China) was slowly added along the wall of the tube without disturbing the pellet, and the sample was stored at 4 °C until it was sent to the laboratory for analysis. Imaging was performed using an electron microscope (HT7700, HITACHI, Japan), and the data were saved for further evaluation.

Culture of primary acinar cells

C57BL/6J mice were sacrificed using CO_2 asphyxiation. Under aseptic conditions, the pancreas was extracted and immersed in sterile PBS. The pancreas was minced to the size of a grain of rice and placed in PBS buffer containing 200 U/mL collagenase IA solution (cat. 11213857001, Roche, USA) and 0.25 mg/mL trypsin inhibitor (cat. T8031, Solarbio, China). It was then digested in an incubator at 37 °C for 18 min.

Afterward, complete medium (Waymouth's medium containing 2.5 % FBS, 1 % Penicillin-Streptomycin mixture (PS), 0.25 mg/mL trypsin inhibitor, and 25 ng/mL recombinant human Epidermal Growth Factor (EGF)) was added to terminate the enzymatic reaction. The digested pancreas was gently agitated, passed through a 100 μm cell filter, and centrifuged at 300 rpm/min for 2 min. The supernatant was discarded, and the pellet was washed three times by adding an appropriate volume of sterile PBS. Isolated acinar cells were then collected, resuspended in complete medium, seeded onto culture plates, and placed in an incubator at 37 °C with 5 % CO2 for culture and further assays.

Measurement of the activity of amylase and lipase

Mouse heart blood was collected and centrifuged at 1000 g for 10 min. Plasma was obtained from the blood by centration at 1000 g for 10 min and stored routinely at −20 °C. Plasma amylase and lipase activities were measured using a clinical analysis system. The amylase activity was measured by EPS substrate assay kit. Lipase activity was measured using a kit for the methyltriazine substrate method, and both were measured using an AU1000 system (Beckman) from the United States.

Immunofluorescent staining of tissues and cells

For immunofluorescence staining of 4-μm paraffin sections of tissue, the sections were placed in an oven at 60 °C for at least 30 min. They were then dewaxed in an immunohistochemical tank while hot, washed with running water, and subjected to peroxidase blocking using 3 % hydrogen peroxide.

Next, 1x original repair enzyme solution was heated to boiling, and the fixed sections were immersed in the solution for 20 min. After cooling to room temperature, the sections were sequentially rinsed with water, distilled water, and PBS. Subsequently, 5 % goat serum (cat. BMS0050, Abbkine, China) was applied to block the sections at room temperature for 30 min. Following this, the serum was removed, and a wet box was used to incubate the sections in a refrigerator at 4 °C overnight.

After incubation, the culture medium was discarded, and the sections were washed twice with PBS. They were then fixed with 4 % paraformaldehyde for 10 min, followed by another wash with PBS. The sections were permeabilized with 0.25 % Triton X-100 (cat. ST1722, Beyotime, China) for 10 min. Finally, 5 % goat serum was added to block the cell slides for 30 min at room temperature, and the primary antibody was applied and incubated at 4 °C overnight. The primary antibody used: ZBP1 (cat. sc-271483, Santa Cruz, USA), GM130 (cat. A25013, Abclonal, China), cleaved-casp3 (cat. 9661, CST, USA), p-MLKL (cat. AF7420, Affinity, China), p-MLKL (cat. 37333, CST, USA), cleaved casp1 (cat. AF4022, Affinity, China), NF-κB (cat. 8242, CST, USA), CD68 (cat. 97778, CST, USA), Ly6G (cat. BP0075-1, Biocell, USA), GOLPH3 (cat. 67777-1-Ig, Proteintech, USA), RIPK3 (cat. sc-374639, Santa Cruz, USA), Amylase (cat. sc-46657, Santa Cruz, USA). The following day, tissue sections and cell slides were processed in a similar manner. The primary antibodies were washed off with PBS, and secondary antibodies were added and incubated in the dark at room temperature for 45 min. After washing off the secondary antibodies with PBS, the nuclei were stained with a DAPI-containing anti-fading reagent (cat. CP36935, Invitrogen, USA). Finally, the sections were sealed, and the results were captured using a confocal fluorescence microscope (Olympus Inc, USA) or a Leica microscope.

Detecting the mitochondrial ROS by MitoSOX red/green staining

Cells were cultured on sterile cell slides, and after the expected treatment, the medium was discarded and the slides were washed with cold PBS. The cell slides were then placed in a wet box. A working solution at 5 μM was prepared according to the Mitochondrial ROS MitoSOX Red kit (cat. M36008, Sigma-Aldrich, USA) and added dropwise to fully cover each slide. The slides were incubated at room temperature in the dark for 20 min.

For tissue staining, Mitochondrial ROS MitoSOX Green (cat. M36006, Sigma-Aldrich, USA) was used, as it demonstrated greater sensitivity than MitoSOX Red in our analysis. A working solution at 10 μM was prepared and applied to each slide containing 10 μm frozen sections, followed by incubation at room temperature in the dark for 30 min.

After incubation, the dye working solution was removed by suction, and the slides were washed twice with PBS for 5 min each time. The excess liquid was drained, and the slides were sealed with a DAPI-containing anti-fading reagent (P36935, Invitrogen, USA). Finally, the results were captured using a fluorescence microscope (Olympus Inc, USA).

Efficacy evaluation of FePTX@CM NPs on SAP mice model

C57BL/6J mice (male, 6–8 weeks old) were purchased from SJA Laboratory Animal Co, LTD (Changsha, China). The experimental animal's use license is SYXK(Xiang) 2022-0012, the experimental animal's production license is SCXK(Xiang)2019-0004, and the batch number of experimental animal production included 430727231101873587, 430,727,231,100,934,318 and 430727231101909167. All mice were randomly divided into 8 groups: Negative control, model group, free PYD, free PTX, free PYD + PTX, FePYD NPs, FePTX NPs, FePTX@CM NPs. Mice were maintained under pathogen-free conditions. The project was approved by the Second Xiangya Hospital of Central South University Ethics Committee and abided by the animal care and use guidelines. Mice were administered different formulations intravenously for the first time, fasted for 12 h, and then intraperitoneally injected with caerulein (cat. S9690, Selleck, Japan) at a dose of 50 μg/kg every hour for a total of 12 injections. After the 6th and 12th injections, mice received intravenous administration of different formulations for the second and third times. After 12 h, the mice were sacrificed, and samples were collected. As a positive control, we administered an anti-Ly6G antibody via intraperitoneal injection (BioXcell BXC-BP0075, 200 μg prior to caerulein administration), which specifically depletes neutrophils in mice and has been consistently demonstrated to exert a significant therapeutic effect in SAP[29,30]. The pancreatic, lung tissues and blood of mice were collected to analyze the severity of the model by detecting the histopathological analysis and the expression levels of plasma amylase and lipase.

For the pancreatic duct ligation-induced SAP model, six to eight-week-old male C57BL/6J mice were used. The mice were fasted overnight and anesthetized using CO_2. A midline incision was made, and the duodenum was gently pulled out to locate the pancreatic duct for ligation. Finally, the incision was sutured closed using an 8–0 suture. Forty-eight hours after ligation, mice received intraperitoneal injections of caerulein (50 μg/kg) at one-hour intervals for a total of two injections. Simultaneously, the mice were administered different formulations for the first time. They also received additional administrations of these formulations over the two days following the modeling. On the second day after the last administration, the mice were sacrificed, and blood, pancreas, and lung tissue were collected for further analysis.

The high mortality observed clinically in SAP is often linked to complications such as uncontrolled sepsis or main organ failure, which may not fully replicate in murine models due to species-specific pathophysiological differences and the course of disease [31]. To uttermost mimic SAP in clinic, the established criteria for validating the SAP mouse model encompass two critical components. The pathophysiological hallmarks include pancreatic injury characterized by necrosis, inflammatory infiltrates, and edema, as well as multi-organ dysfunction manifesting as systemic complications such as acute lung injury, renal impairment, or intestinal barrier compromise [32]. Additionally, biochemical markers demonstrate significant elevation of blood amylase and lipase levels (≥3 times the upper limit of normal) [33]. In this study, we employed two distinct mouse models of SAP to evaluate the therapeutic efficacy of our newly developed nanoparticle-based drug.

ELISA assay for IL-1β and IL-6 in plasma or cell supernatants

Mouse heart blood was collected and centrifuged at 1000 g for 10 min. Plasma was obtained without disturbing the cell pellet and routinely stored at −20 °C. The expression levels of IL-1β and IL-6 in the plasma or cell supernatants were detected using the IL-1β and IL-6 ELISA Kits (RK00006 and RK00008, Abclonal, China) according to the manufacturer's instructions.

TUNEL assay

After fixing the tissue with 4 % formaldehyde, it was embedded in paraffin and cut into 4 μm sections. The sections were placed in an oven at 60 °C for 60 min, followed by dewaxing and washing with distilled water for 5 min. A 20 μg/mL proteinase K solution (cat. ST535, Beyotime, China) was added dropwise and incubated at 37 °C for 15 min. The samples were then washed three times with PBS, with each wash lasting 5 min.

Next, a TUNEL reaction mixture (cat. C1086, Beyotime, China) was added dropwise and incubated at 37 °C in the dark for

60 min, followed by three washes with PBS. DAPI staining was then applied, and the slides were sealed with nail polish. Image acquisition was performed using a fluorescence microscope (Olympus Inc, USA).

H&E staining

After dewaxing the sections as described in the previous steps, they were immersed in hematoxylin staining solution for 5 min, then differentiated with 1 % hydrochloric acid alcohol for a few seconds and rinsed with tap water for 5 min. The sections were subsequently treated with warm water to enhance the bluing effect.

Next, they were placed in eosin staining solution for 1 to 3 min, rinsed again with tap water for 5 min, and then dehydrated and dried. After sealing with neutral resin, the sections were examined under a microscope (ZEN, Germany) for image acquisition and data analysis.

Ethics statement

Animal experiments were performed according to the protocols approved by the Second Xiangya Hospital of Central South University Ethics Committee and abide by the animal care and use guidelines (No. 20230897).

Statistical analysis

Data were presented as mean ± SD. Statistical analysis was performed by GraphPad Prism (9.5.0). T-test was used for comparison between two groups. One-way ANOVA using the Tukey post-test was applied for comparison among three or more groups. The number of replicates is indicated in the legend of each figure.

Results and Discussion

Proanthocyanidin inhibits the release of pancreatic amylase and lipase

Severe acute pancreatitis (SAP) is often characterized by the self-digestion of pancreas mediated by over-released pancreatic enzymes including amylase and lipase in patients [34]. Herein, the inhibition of these enzymes is of great significance to relieve clinical symptoms and provide better prognosis. During our screening of various natural compounds and their derivatives for SAP, proanthocyanidin (PYD) exhibited an exciting capacity for anti-inflammation and anti-release of pancreatic enzymes. As shown in Fig. S1A, AR42J cells were pre-treated with dexamethasone (Dex) at day 0 to polarize toward exocrine phenotype. In control group, the fluorescence signal of intracellular amylase was hard to observe because they were secreted to extracellular spaces. After PYD intervention (50 μg/ml) from day 1, the signal of amylase was located in cytoplasm more in day 2 and day 4. The statistical analysis revealed that PYD effectively inhibited amylase release though in exocrine phenotype cells. Conversely, the level of amylase and lipase in cell supernatant after PYD treatment decreased as expected in Fig. S1B. To further elucidate the specific process of enzyme-release inhibition by PYD, we detected the intracellular RNA level of both enzymes. The results demonstrated that there were no significant differences between control and PYD groups, which meant PYD influenced the release stage rather than the transcription process of amylase and lipase (Fig. S1C and Fig. S1D). We also verified the protection effect of PYD in primary acinar cells. As depicted in Fig. S1E, mice were pre-treated with PYD for a week before acinar cell isolation. The acinar cells were then stimulated by caerulein to create damaged state. The cell supernatants of post-stimulated acinar cells were isolated for amylase and lipase detection. After caerulein treatment, the level of pancreatic enzymes in control group increased significantly, while PYD-treated group excitingly decreased enzymes secretion (Fig. S1F). The protection effect of PYD in pancreatic enzyme release was confirmed via these experiments. Considering its anti-inflammation property in reports, the potential of PYD in anti-SAP encouraged us to further develop its novel formulations to better target the pancreas and evade MPS.

Preparation and characterization of FePYD@CM and FePTX@CM NPs

The ability of polyphenol molecules to coordinate with metal ions such as Fe^{3+}, Cu^{2+}, etc. to form nanoparticles was reported by lots of studies. Therefore, the polyphenol structure of PYD could react with iron ions (III) to prepare nanoparticles (NPs). To further enhance pancreas-targeting ability of NPs, we wrapped the NPs with macrophage cell membranes (CM). It is reported that the biomolecular-directed assembly is a promising pathway to prepare stable metal-polyphenol NPs because they offer effectively strong and stable bonding specificity. We used PEG10000 as the seeding agent for the assembly to locally increase the concentration of Fe^{3+}, PYD and biomacromolecules (BSA). As shown in Fig. 2A, the particle size FePYD NPs (167.6 ± 1.2 nm) was smaller than that of FePYD@CM NPs (185.2 ± 3.0 nm). And the NPs sizes were stable in 2 weeks with a homogenous polydispersity index (PDI) (Fig. 2B). Also, FePYD@CM NPs were stable in different solvents as shown in Fig. S2A. The zeta potential results demonstrated positive charge for both NPs (Fig. 2C). After cell membrane (CM) coating, the zeta potential of FePYD@CM NPs decreased by about 10 mV which may be attributed to the neutralization effect of negative charge of CM. Furthermore, the morphology of FePYD@CM NPs was investigated by TEM. It could be observed that a significant cell membrane layer coated on the FePYD NPs, approximately 10 nm (Fig. 2D). Elemental mapping analysis revealed the co-localization of phosphorus in the NPs, which indicated the existence of cell membrane (Fig. 2E). Also, we adopted Coomassie blue staining to investigate the total protein of different formulations. As expected, FePYD@CM group showed the same protein profile as original cell membrane group (Fig. 2F). And UV-absorbance spectrum of FePYD@CM was investigated as shown in Fig. 2G. The characteristic peak of PYD existed in both NPs with or without CM coating. Additionally, the CM coating efficiency of NPs was determined by nano-flow cytometry. First, DiL was used to label CM. Centrifugation was performed to remove unbound DiL. And then nano-flow cytometry was utilized to analyze the encapsulation efficiency of CM on FePYD NPs. The result showed that the encapsulation rate of CM on FePYD@CM NPs was around 81.7 %, indicating that most FePYD NPs were wrapped by macrophage membranes (Fig. 2H). Considering the self-assembly property of FePYD NPs, we used different interference agents including urea, NaCl, SDS to investigate the specific interaction forces during the assembly process. The particle size varied after the addition of different agents (Fig. 2I). It was significant that after NaCl interference the NPs disassembled, while SDS also exhibited little impact on particle size. Conversely, urea did not significantly influence NPs assembly, which suggested that the hydrogen bond may be not the main force working in NPs formation. Accordingly, electrostatic force and hydrophobic interaction were the main factors in NPs assembly. Moreover, the drug release profile of FePYD@CM NPs in Fig. S3 demonstrated that the NPs could release PYD over 50 % within 24 h to achieve sustained drug release, avoiding systemic cytotoxicity and prolonging efficacy.

Cellular uptake and pancreas targeting ability of FePYD@CM NPs

The alleviation of SAP required the drugs to be uptake sufficiently and quickly into related cells in inflammation-microenvironment. Therefore, we investigated the cellular uptake

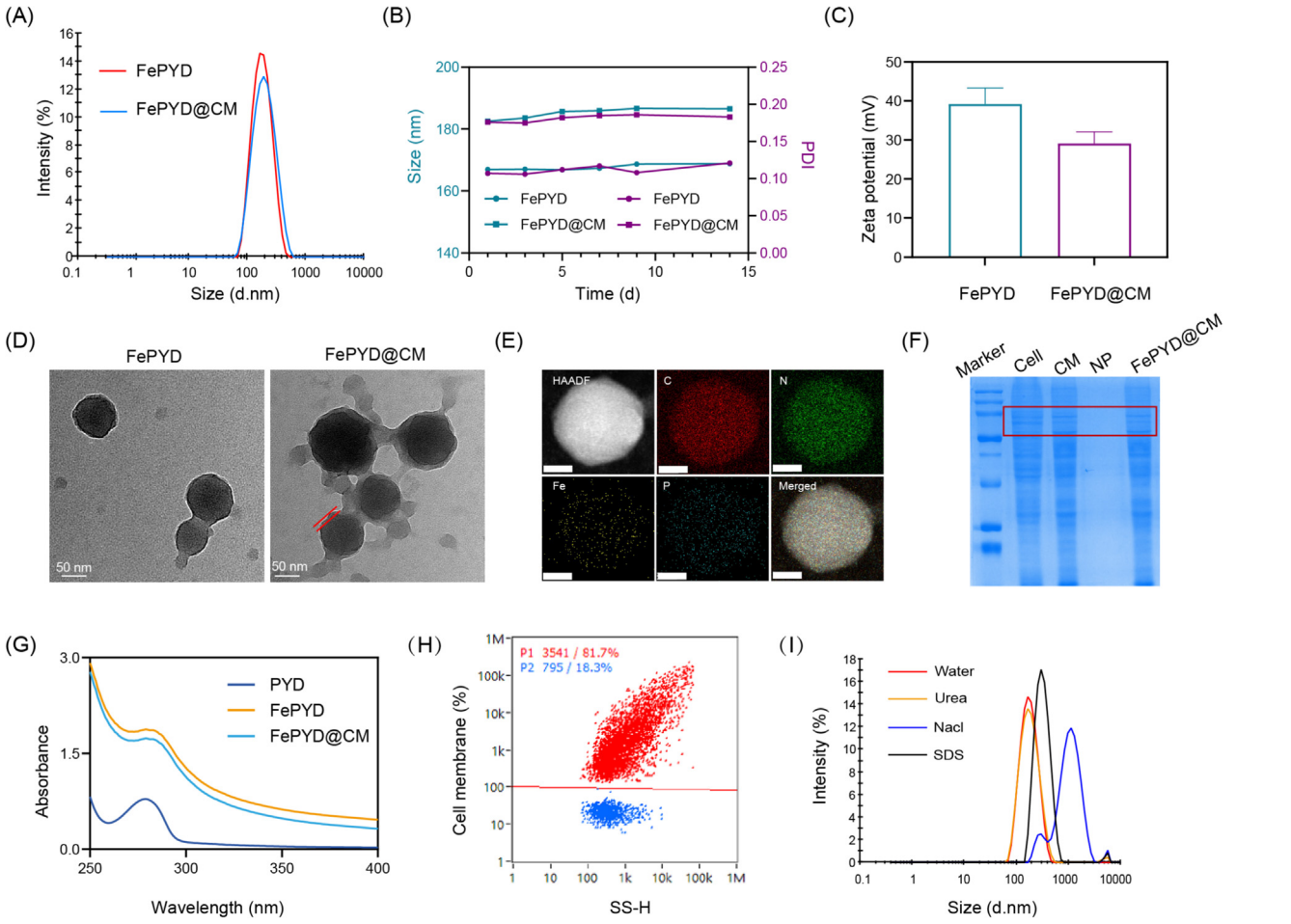

Fig. 2. Preparation and characterization of FePYD@CM NPs (n = 3). (A) Size distribution of FePYD@CM NPs. (B) Size stability evaluation of FePYD@CM NPs. (C) Zeta potential of FePYD@CM NPs. (D) TEM images of FePYD@CM NPs. Scale bar = 50 nm. (E) Elemental mapping of FePYD@CM NPs. Scale bar = 10 nm. (F) Total protein profile of FePYD@CM NPs. (G) Ultraviolet absorption spectrum profile of FePYD@CM NPs. (H) Evaluation of encapsulation efficiency of CM on FePYD NPs by nano-flow cytometry. (I) Particle size change of FePYD@CM NPs after the addition of different agents. Data = mean ± SD.

of FePYD@CM NPs in vitro. RAW264.7 and 266-6 cell lines were used to simulate the main cells concentrated in SAP microenvironment. Results of fluorescent microscopy and flow cytometry suggested that FePYD@CM were internalized much more into cytoplasm than free DiL dye and FePYD without cell membranes in both cell lines (Fig. 3A to 3F). This may be attributed to the positive charge of the NPs and homogeneity of macrophage membranes. The similarity of CM on our NPs and macrophage membrane promoted their fusion and co-localization. However, it is not persuasive enough to investigate the uptake of our NPs only in cellular level. We wondered whether the FePYD@CM NPs could target pancreas in vivo to bring therapeutic effects within 24 h. The fluorescent images of in vivo imaging system (IVIS) demonstrated that a significant increase distribution of FePYD@CM NPs in pancreas when in comparison to free DiR and FePYD NPs (Fig. 3G and 3 J). Meanwhile, the excised pancreas in FePYD@CM group showed more evident fluorescence than the other two groups (Fig. 3H and 3 K). However, the signal of both NPs was also observed in liver, spleen and lung (Fig. 3I and 3L). We speculated that the positive charge of NPs attracted the MPS to devour them in these organs which was inevitable. After macrophage membrane coating, FePYD@CM NPs exhibited better pancreas targeting ability than FePYD NPs due to the CM homogeneity. Either way, our FePYD@CM NPs are more precise in pancreas targeting within 24 h, thereby providing rapid relief for SAP.

Furthermore, we conducted the biosafety assessment of FePYD@CM NPs by the hemolysis test, the serum level of ALT, AST, BUN, CR and the H&E staining of major organs. Considering the administration manner, the primary issue was whether the formulation could induce hemolysis when first entered the blood circulation. The results in Fig. S4A indicated that there was no significant erythrocyte lysis, even at a concentration of 500 μg/ml for FePTX@CM NPs. Also, the serum level of the serum factors which indicated the function of liver and kidney fluctuated in normal range (Fig. S4B). Furthermore, the images of H&E staining suggested that there was no significant damage in major organs including heart, liver, spleen, lung and kidney (Fig. S4C). Collectively, the biosafety investigation experiments demonstrated that our NPs were safe enough to administer intravenously.

PYD inhibits mitochondrial ROS/Golgi stress-mediated pancreatic digestive enzymes secretion

When SAP occurs, the acinar cells become stressed, leading to the production of reactive oxygen species (ROS) in cytoplasm, especially in mitochondria (mtROS). Excess accumulation of mtROS is a key initiator that induces inflammation, lipid peroxidation, protein oxidation, and DNA damage. We first used MitoSOX Red to visualize mtROS inside 266-6 cells following taurocholic acid sodium (TAC) intervention, which was used to mimic acinar

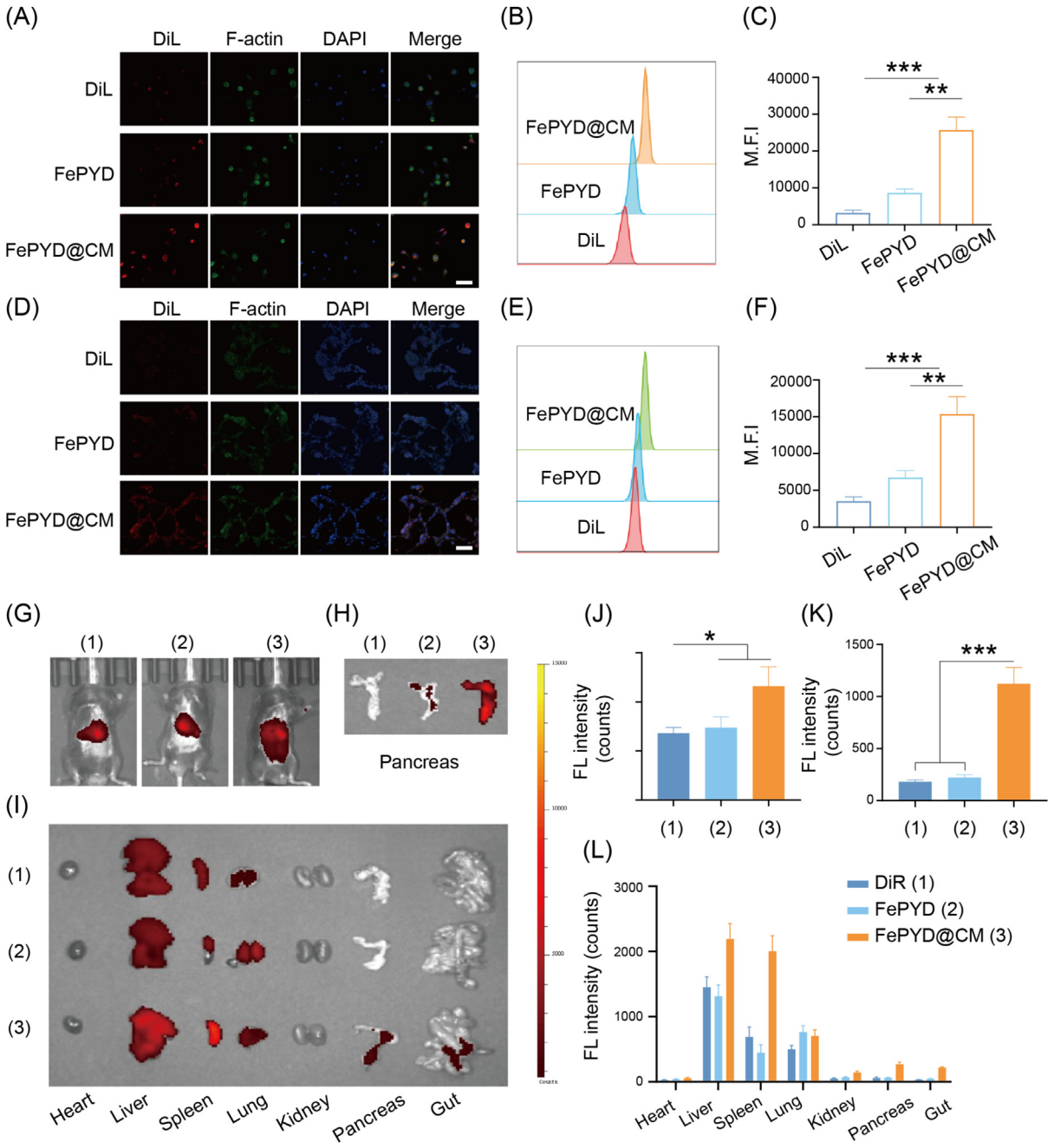

Fig. 3. Evaluation of cellular uptake and pancreas targeting ability of FePYD@CM NPs. (A) Fluorescent images of cellular uptake of FePYD@CM NPs in macrophages (n = 3). Scale bar = 100 μm. (B-C) Flow cytometry analysis of cellular uptake of FePYD@CM NPs in macrophages (n = 3). (D) Fluorescent images of cellular uptake of FePYD@CM NPs in 266-6 cells (n = 3). Scale bar = 100 μm. (E-F) Flow cytometry analysis of cellular uptake of FePYD@CM NPs in 266-6 cells (n = 3). (G) In vivo fluorescent images of mice received different formulations and its analysis (J). (H) Fluorescent images of excised pancreas of each group and its analysis (K). (I) Fluorescent images of ex vivo organs after different interventions and its analysis (L). *P < 0.05, **P < 0.01, ***P < 0.001. Data = mean ± SD.

cell damage during SAP. TAC-induced mtROS production was dosage-dependent as shown in Fig. S5A. MitoQ is an antioxidant agent that can repair oxidative damage to mitochondria within cells. We isolated the primary acini to simulate SAP situation with caerulein. As shown in Fig. S5B, mitoQ could significantly decrease the intracellular mtROS though caerulein existed. Next, mitoQ exhibited obvious amylase and lipase release-inhibition effects in primary acinar cells (Fig. S5C). Therefore, we demonstrated that mtROS promotes the release of amylase and lipase, resulting in subsequent pancreatic dysfunction. To further investigate the anti-enzyme secretion effect of FePYD@CM NPs, 266-6 cells were co-treated with FePYD@CM NPs and TAC. Fig. S5D demonstrated significant mtROS production after TAC stimulation. Free PYD could reduce mtROS level, while FePYD@CM NPs exhibited the best anti-mtROS effect. Furthermore, the addition of rotenone was used to reverse mtROS levels and validate the mechanism by which it abolishes the anti-mtROS and anti-enzyme release effects of FePYD@CM NPs observed in 266-6 cells, as depicted in Fig. S5D and Fig. S5E. We then observed the amylase and lipase release in primary acini which received caerulein treatment (Fig. S5F). The results further confirmed that pancreatic enzymes release was dependent on the level of mtROS. After intervention with PYD or FePYD@CM NPs, the levels of amylase and lipase in the cell supernatant significantly decreased, with FePYD@CM NPs demonstrat-

ing better uptake efficiency and a more pronounced suppression of enzyme release; however, this effective inhibition was reversed by rotenone intervention.

Meanwhile, Golgi stress was important in mtROS-mediated cell dysfunction. GM130 and GOLPH molecules are the main proteins responsible for maintaining the function and structure of Golgi. First, we found a significant signal of GM130 in TAC-treated 266-6 cells (Fig. S5G). When compared to control group, the structure of Golgi apparatus was irregular and broken in TAC-treated cells. The situation of fractured Golgi could be improved by PYD and FePYD@CM NPs. Particularly, better status of Golgi was inspected in NPs group. Further, the co-localization of GOLPH3 (key functions in vesicle transport and maintaining the integrity of the Golgi apparatus) and GM130 in Fig. S5H revealed the impaired integrity of Golgi apparatus with TAC treatment. As expected, PYD and FePYD@CM NPs showed attractive inhibition in Golgi structure damage and improvement of Golgi integrity. On the other hand, the Golgi stress could be reflected by relevant expression of certain proteins including SIRT2 and glycosylated MUC2. Western Blot images in Fig. S5I showed that PYD has the potential to reduce the levels of both proteins and enhance cellular amylase within cells, indicating alleviated Golgi stress and preventing the release of amylase, whereas Brefeldin A (BFA), a specific inducer of Golgi stress, completely abolished its therapeutic effect in 266-6 cell lines. Furthermore, amylase in primary acinar cell supernatant decreased after PYD and FePYD@CM NPs treatment in caerulein-induced SAP in vitro (Fig. S5J). The inhibition effect of BFA towards both formulations verified the Golgi stress pathway was indeed involved in pancreatic enzyme release.

Accordingly, the mechanisms of PYD or FePYD@CM NPs-inhibited amylase and lipase release were associated with mtROS/Golgi stress pathway, thereby minimizing the autolysis of pancreatic tissues in SAP.

Pentoxifylline formulations inhibit macrophage PANoptosis via the Zbp1 pathway

Macrophages play an important role in SAP initiation and development. Excessive macrophage pro-inflammatory cell death (including pyroptosis, necroptosis and apoptosis) releases numerous pro-inflammatory cytokines to amplify SAP response. Maintaining the survival of macrophages is of great significance for controlling SAP response, preventing systemic reaction and tissue protection. Using novel drugs to protect macrophages from pro-inflammatory cell death is a reliable strategy in SAP therapy. Reports confirmed that Pentoxifylline (PTX) exhibited multiple functions in SAP treatment including anti-inflammation and neutrophils inhibition, etc. Here, we explored whether PTX could protect macrophages from activation or pro-inflammatory cell death in SAP. First, to better develop the classic PTX in the clinic, we loaded PTX into FePYD and FePYD@CM NPs to prepare FePTX and FePTX@CM NPs for multifunctional treatment. The effective components of FePTX@CM NPs were PYD and PTX. And drug loading efficiency was 23.07 ± 1.83 % and 4.875 ± 0.36 %, respectively (Fig. S6). Subsequently, we isolated bone marrow-derived macrophages (BMDMs) to simulate macrophages by LPS and conducted transcriptome analysis following different interventions to explore the impact of PTX on the activation of macrophages (Fig. 4A). Treatments administered to BMDMs included LPS, LPS + PTX, LPS + FePTX NPs, LPS + FePTX@CM NPs. According to the gene set enrichment analysis (GSEA) results in Fig. 4B to 4C, several classic proinflammation genes were enriched in LPS treated BMDM indicating classic proinflammatory signal pathway were regulated by LPS in BMDMs. Compared to LPS, the PTX treatment led to the enrichment of multiple inflammation regulation pathway in BMDMs (Fig. 4D-E). Specifically, the expression of various pro-inflammatory factors such as IL-1β and IL-6 were decreased and anti-inflammatory factors such as IL-10 increased after PTX formulation interventions (Fig. 4F). IL-1 is a major cytokine that appears in the early stages of inflammation, especially during the initial phase of SAP. IL-6 can further directly reflect the severity of the disease. This evidently proved that PTX and its formulations (including FePTX, FePTX@CM NPs) downregulated pro-inflammatory pathway in BMDMs, thereby exerting an exciting inflammation inhibition effect to relieve SAP. The results were re-verified by qPCR analysis that expression of IL-1β and IL-6 induced by LPS were decreased by 80 % and 62 % by FePTX and FePTX@CM NPs, respectively (Fig. 4G). To investigate the potential mechanism of PTX and its nanoformulation in macrophage suppression, we first conducted a CCK-8 assay to evaluate cell viability and assess the potential for suppressing pro-inflammatory cell death. As shown in Fig. 4H, PTX formulations prevented BMDMs from death, especially when it was presented in nanoparticles. The protection effect was also confirmed by propidium iodide (PI) staining in Fig. 4I. Thus, the significant cell death induced by LPS was alleviated by both free PTX and NPs, which, based on previous reports, can explain why PTX and NPs are able to suppress macrophage activation.

Recent advances suggest that several pro-inflammatory cell death pathways share the same initiation mechanism, known as PANoptosis, which is characterized in macrophages by cell swelling, membrane rupture, and the release of pro-inflammatory factors. To further investigate the molecular mechanisms underlying PTX intervention in LPS-triggered macrophage cell death, we performed a western blot assay to evaluate the level of various PANoptosis biomarkers, including cleaved caspase 1 (pyroptosis), p-MLKL (necroptosis), p-RIPK3(necroptosis), cleaved caspase 9 (apoptosis), etc. As shown in Fig. 3JI, the images indicate that LPS induced the overexpression of all relevant PANoptosis biomarkers, demonstrating its activation in BMDMs; however, treatment with PTX and FePTX@CM NPs significantly inhibited the PANoptosis process, as evidenced by the decreased expression of these biomarkers (Fig. 4J). Intuitive observation of BMDMs morphology via transmission electron microscope (TEM) was conducted then. The LPS-induced typical appearance change of pyroptosis, apoptosis and necroptosis was evidently observed and analyzed in Fig. 4K. The FePTX@CM NPs greatly alleviated the PANoptosis of BMDMs. The death process was limited by FePTX@CM NPs to the early death stage or primed to autophagy for self-protection. Therefore, we predicted that FePTX@CM NPs suppressed the macrophage PANoptosis process induced by LPS which was common in SAP stages. The reason why FePTX@CM NPs exhibited better anti-PANoptosis effects than free PTX may be attributed to their better cellular uptake. Behind this phenomenon, we found that the PANoptosomes assembly was influenced by FePTX@CM NPs in co-immunoprecipitation (co-IP) assay (Fig. 4L). The innate immune sensor Zbp1 is one of the specific upstream molecules involved in the process of PANoptosis. It can sense specific stimuli and trigger the assembly of the PANoptosomes. Additionally, RIPK3 and caspase 6 were the other two crucial components of PANoptosomes. According to Fig. 3L, FePTX@CM NPs significantly decreased the Zbp1 and RIPK3 interaction in macrophages, along with the decrease of RIPK3 and caspase6 in RIPK3 antibody immunoprecipitated pool, indicating an obvious suppression of PANoptosomes assembly in macrophages, thus inhibiting PANoptosis. These results enlightened us to further explore the role of Zbp1 molecule in PANoptosis-suppression effect of PTX in SAP therapy.

We extracted the PANoptosis-related genes of transcriptomics in BMDMs to generate the heatmap after LPS and PTX formulation intervention to visualize the expression PANoptosis regulators including Zbp1, RIPK1, NRPL3, caspase3, caspase 6, caspase 8 and MLKL, as shown in Fig. 5A. Compared to control group, only Zbp1

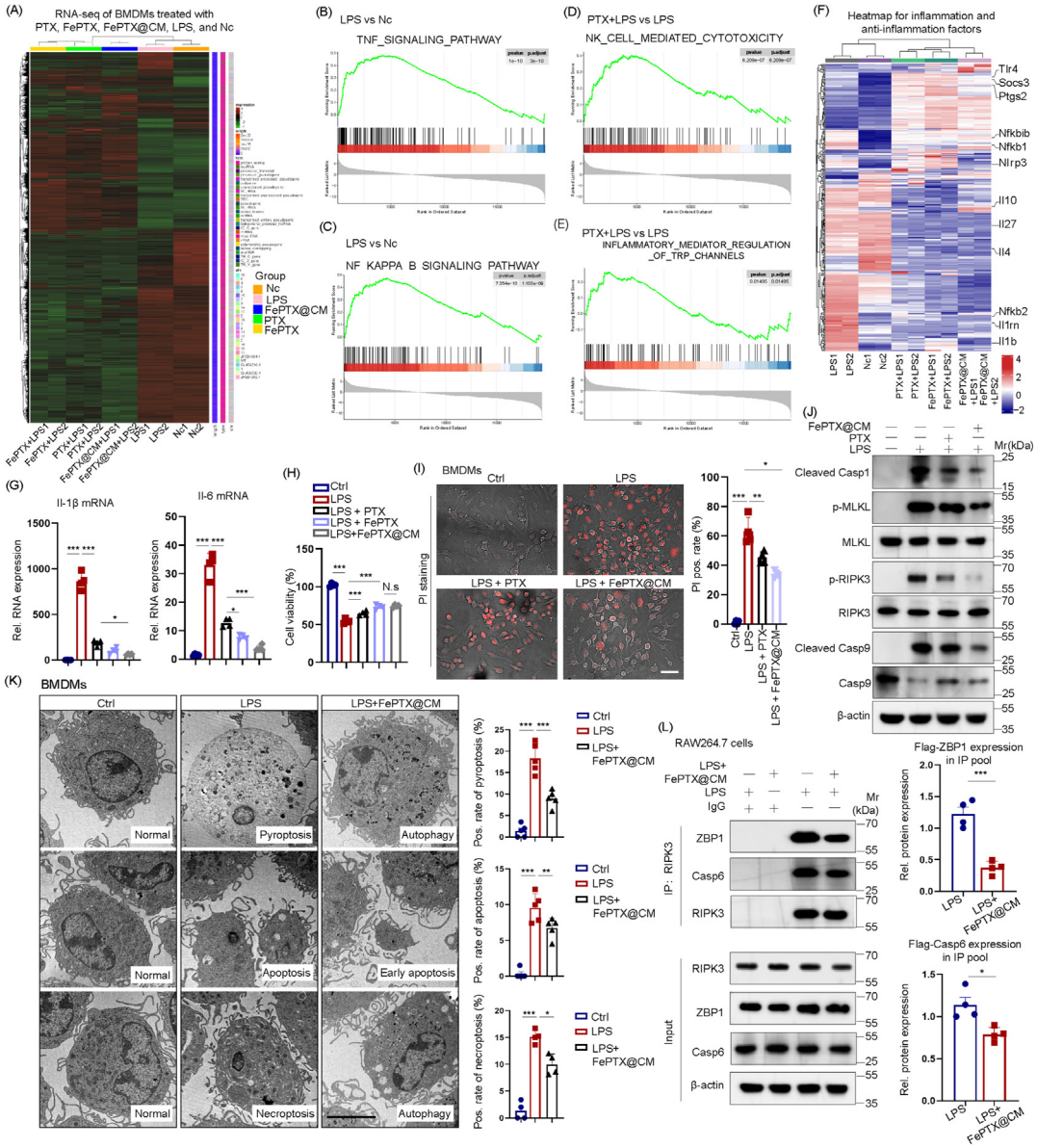

Fig. 4. PTX formulations inhibited macrophage PANoptosis. (A) Gene clustering analysis of PTX, FePTX, FePTX@CM-treated BMDMs. (B-C) GSEA analysis of transcriptomics results of BMDMs after LPS intervention. (D-E) Inflammatory-related pathway analysis in transcriptomics results of BMDMs after different PTX formulation interventions. (F) Heatmap of transcriptional profiling of inflammatory factors in BMDMs after PTX formulation interventions. (G) Results of qPCR sequencing (n = 4). (H) Cell viability of BMDMs with different treatments (n = 4). (I) PI staining images of BMDMs after LPS and FePTX@CM NPs treatment and its analysis (n = 4). Scale bar = 100 μm. (J) WB detection of the PANoptosis biomarkers in BMDMs upon treatment with FePTX@CM NPs. (K) TEM images of BMDMs after different treatments. Scale bar = 5 μm. (L) Co-IP analysis of PANoptosomes biomarkers in RAW264.7 after various interventions (n = 4). *P < 0.05, **P < 0.01, ***P < 0.001, N.s. = no significance. Data = mean ± SD.

and RIPK1 genes upregulated significantly in LPS group, whereas PTX and its formulations remarkably downregulated their expression, particularly that of Zbp1. The qPCR was further performed to evaluate the relative RNA level of the PANoptosis upstream gene Zbp1 (Fig. 5B). In the LPS-treated group, RNA of Zbp1 increased by 8.4 times while in the PTX, FePTX, and FePTX@CM NPs-treated groups, it only increased by factors of 4.3, 2.2, and 1.7 respectively. Previous studies have established that Zbp1 expression may be modulated by microRNAs (e.g., miR-99b-5p) [35], epigenetic modifications [36], and transcription factors such as HSF1 [37]. In our current study, we demonstrated that PTX downregulates Zbp1 expression at both RNA and protein levels; however, our findings do not preclude the potential involvement of the aforementioned regulatory pathways.

These findings suggest that FePTX@CM NPs may inhibit the initiation stage of PANoptosis in BMDMs by downregulating Zbp1. Immuno-fluorescence assay provided an intuitive way to observe the Zbp1 expression in BMDMs whose results were in consistent with previous statement (Fig. 5C). Then we applied adenovirus to overexpress Zbp1 in macrophage. co-IP results revealed the Zbp1-overexpressed macrophages reversed the PANoptosis-inhibition effect of FePTX@CM (Fig. 5D). The interactions between Zbp1 and RIPK3 in LPS and Zbp1 oe-group were significantly enhanced due to the existence of numerous Zbp1. And the protection effect of FePTX@CM was weakened by excessive Zbp1. Reports declaimed that Zbp1 interacted with RIPK3 to elicit the formation of PANoptosomes and execution phase of PANoptosis. Thus, we investigated the co-localization of Zbp1 and RIPK3 via fluorescent microscope (Fig. 5E). It was obvious to observe that FePTX@CM NPs minimized the co-localization of the two proteins which means the assembly of PANoptosomes was restricted as much as possible with PTX formulations interventions. In all the experi-

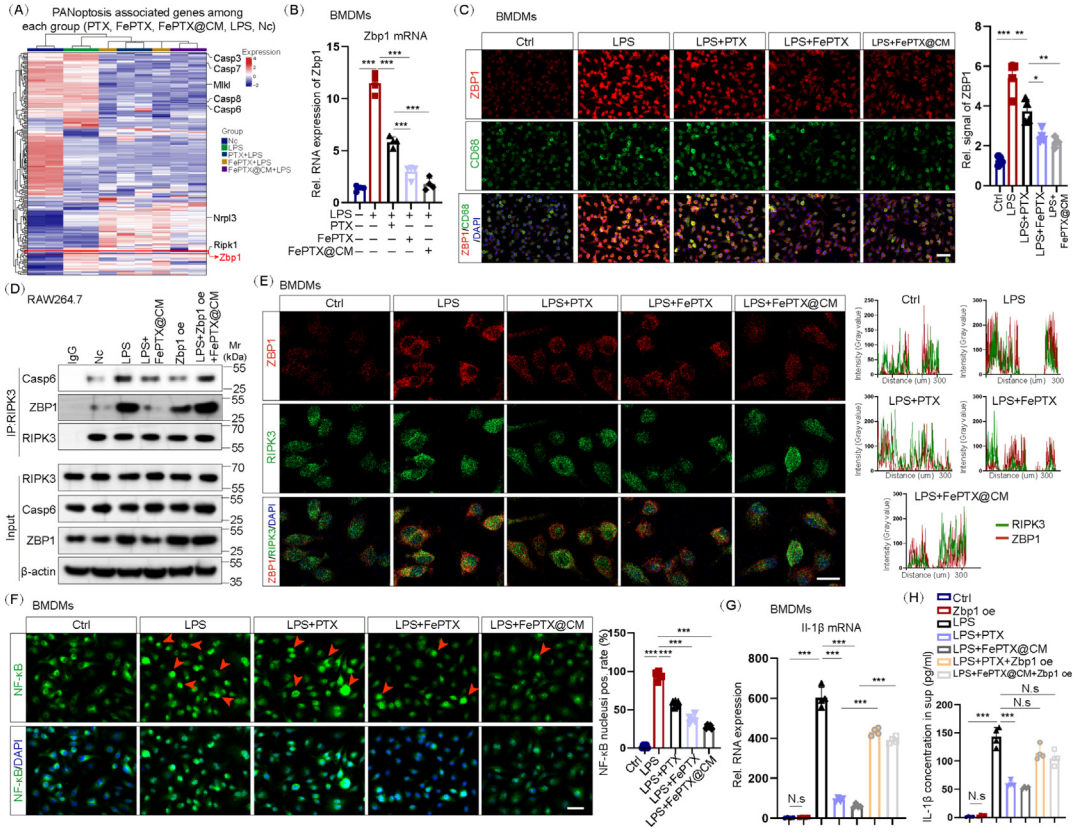

Fig. 5. PTX and its formulations could effectively inhibit Zbp1-mediated PANoptosis of BMDMs. (A) Heatmap of PANoptosis associated genes among each group. (B) qPCR analysis of Zbp1 in each group after various interventions (n = 4). (C) Fluorescent images of Zbp1 in BMDMs and its statistic graph. Scale bar = 100 μm. (D) Co-IP images of PANoptosis biomarkers after various treatments involving Zbp1-overexpressed macrophages. (E) Fluorescent co-localization images of Zbp1 and RIPK3 in BMDMs of each group. Scale bar = 15 μm. (F) Fluorescence images of NF-κB expression and localization in BMDMs in each group. Scale bar = 50 μm. (G) Results of qPCR and ELISA assay of IL-1β in Zbp1-overexpressed BMDMs after various interventions (n = 4). *P < 0.05, **P < 0.01, ***P < 0.001, N.s. = no significance. Data = mean ± SD.

ments mentioned above, the group treated with FePTX@CM NPs consistently showed the lowest level of Zbp1. On the other hand, NF-κB was a key transcription factor involved in inflammatory activation after initiation of PANoptosis in macrophages [38]. Results of Immuno-fluorescent assay showed that the expression of NF-κB was downregulated and primarily located in cytoplasm rather than nucleus after FePTX@CM NPs treatment, which means the downstream inflammatory responses were limited (Fig. 5F). This may be attributed to the highly homologous and biocompatible cell membrane coated on the surface of FePTX, which resulted in a significant uptake by BMDMs. Furthermore, we found that IL-1β (the main proinflammatory factor) expression was also constrained by PTX-related NPs via qPCR and ELISA assays. However, the Zbp1-overexpressed BMDMs significantly exhibited higher IL-1β levels, which nearly reversed the effect of PTX nanoparticles (Fig. 5G-H). This means the cytokine release was the downstream response of Zbp1 activation. Accordingly, we speculated the PANoptosis of BMDMs induced by LPS was mediated by Zbp1, whereas PTX and its NPs formulations could obviously suppress the expression of Zbp1, resulting in disruption of PANoptosome assembly and alleviation of PANoptosis.

This discovery allows us to utilize FePTX@CM NPs for suppressing macrophage activation in the treatment of SAP.

Efficacy of FePTX@CM NPs against SAP in mice models

The final purpose of our FePTX@CM NPs was to handle clinical SAP. We established two SAP models to reflect clinical situations induced by different factors.

Caerulein is a peptide analog of cholecystokinin (CCK). It can stimulate the pancreas to induce a large secretion of pancreatic enzymes, leading to autolysis of pancreatic acinar cells. The activity of pancreatic enzymes and inflammation further activates a series of cellular damage. The advantage of caerulein in establishing an SAP model lies in its relative simplicity, minimal surgical trauma, low cost, and rapid generation of SAP.

To better assess the efficacy of active ingredients in NPs, we set up eight groups including negative and model group, free PYD, free PTX, free PYD + PTX, FePYD NPs, FePTX NPs, FePTX@CM NPs. According to the drug loading ratio of PYD and PTX in FePTX@CM NPs, we set the drug ratio of PYD to PTX at 5:1 (PYD 5 mg/kg, PTX 1 mg/kg). To evaluate the efficacy of our NPs, we also set up a positive control group, which was administered an anti-Ly6G antibody via intraperitoneal injection to deplete neutrophils in mice (Fig. S8). Generally, SAP was characterized by widespread necrosis of the pancreatic acinar cells and remote organ damage (such as the lung and intestine). The cell morphology of pancreas could effectively reveal the severity of SAP. As depicted in Fig. 6A and Fig. S1B, compared to the negative group, the H&E staining images of model group exactly showed typical necrotizing pancreatitis changes in the caerulein-treated pancreas, including the destruction of structure, massive cell edema and necrosis and infiltration of inflammatory cells, while positive control group exhibited significantly attenuated pathological changes. The lung tissue damage was also observed obviously in positive control group due to the systemic inflammatory responses. In drug-administered groups, the damaged pancreatic tissue has been improved to varying degrees and the images demonstrated that

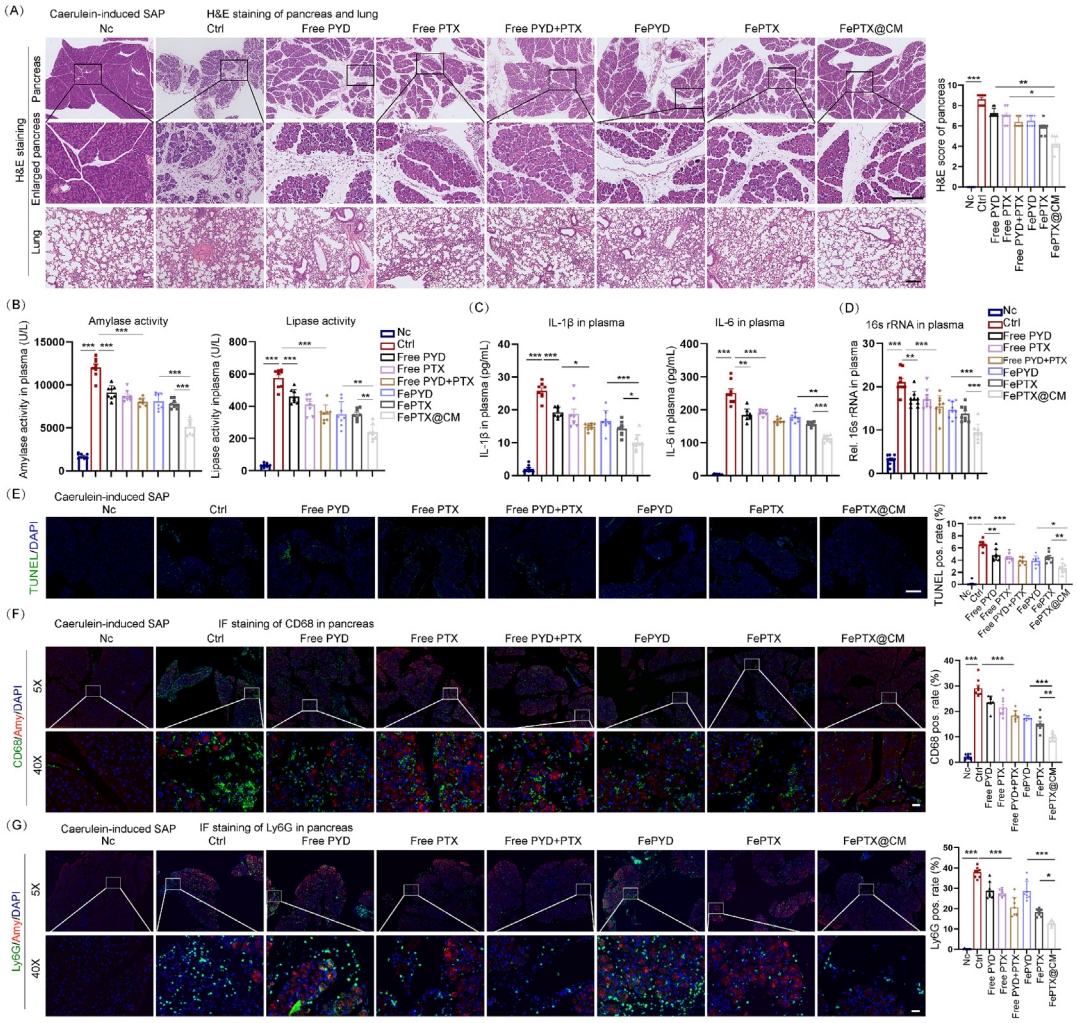

Fig. 6. Efficacy of FePTX@CM NPs in caerulein-induced SAP model. (A) H&E staining images of pancreas and lungs with different interventions and statistical analysis (n = 8). Scale bar = 200 μm. (B) Amylase and lipase activity in plasma of each group (n = 8). (C) Plasma level of IL-1β and IL-6 of each group (n = 8). (D) Result of 16 s rRNA in plasma of each group (n = 8). (E) TUNEL images and analysis of each group after treatments (n = 8). Scale bar = 100 μm. (F-G) Fluorescent images of the co-localization of macrophages and neutrophils in pancreas after various interventions (n = 8). Scale bar = 25 μm. *P < 0.05, **P < 0.01, ***P < 0.001. Data = mean ± SD.

FePTX@CM NPs exert the best therapeutic effect with much alleviated damage and less infiltrated inflammatory cells in pancreas and lung tissue. According to the H&E score of the pancreas, the free drug showed a reduced anti-SAP effect due to its poor pancreas-targeting ability, while treatment with FePTX@CM NPs demonstrated significantly enhanced protective effects on the pancreas in SAP. We then investigated the plasma level of amylase, lipase and pro-inflammatory cytokines. Amylase and lipase activity in plasma was minimized by FePTX@CM NPs compared to other formulations (Fig. 6B, Fig. S1C). Free PTX or PYD demonstrated an obvious enzyme-inhibition efficacy as well owing to their innate anti-inflammatory property in the microenvironment. Similarly, the level of main proinflammatory factors such as IL-1β and IL-6 in plasma also decreased after different interventions (Fig. 6C). Interestingly, a significant difference in amylase and lipase activity was observed between the FePTX NPs and FePTX@CM NPs groups, which may be attributed to the cell membrane coating on the FePTX@CM NPs enhancing their biocompatibility and cellular uptake efficiency. Thus, the results hinted that the organ damage and local and systemic inflammatory response were effectively inhibited by FePTX@CM NPs therapy in SAP model. In addition, Research has found that intestinal barrier dysfunction is a critical characteristic of SAP, leading to increased mucosal permeability and allowing the entry of intestinal microbiota into the bloodstream, ultimately resulting in septicemia [39]. To examine the therapeutic effect of these formulations on intestinal barrier dysfunction in SAP, we evaluated the migration of intestinal bacteria into the circulation through 16S rRNA detection. The results showed a significant decrease in bacterial content in FePTX@CM NPs group in comparison with other formulations (Fig. 6D). Moreover, the total cell death of pancreas was assessed by TUNEL staining in mouse model (Fig. 6E). The positive signal indicated dead cells, which was significantly reduced in FePTX@CM NPs group. Macrophages (especially M1 type) and neutrophils were the key pro-inflammatory immune cells infiltrating the pancreas, and our NPs significantly reduced their infiltration in SAP (Fig. 6F and 6G). The statistical analysis all revealed the best efficacy of FePTX@CM NPs against SAP than single drugs or FePTX NPs. We speculated that FePTX@CM NPs better targeted pancreas and functioned in SAP by alleviating death of acinar cells, relieving pro-inflammation response thus decreasing pathological damage in pancreas and remote organs. In general, FePTX@CM NPs have effectively exerted a protective effect on the caerulein induced-SAP model.

As mentioned above, the caerulein-induced SAP primarily mimics SAP caused by biliary, alcoholic, or other factors leading to pancreatic hyperstimulation and abnormal enzyme activation. Another SAP model was established by pancreatic duct ligation

to simulate pancreatic duct obstruction by biliary stone in the clinic. Differing from caerulein-induced SAP, the pathological changes in H&E images of duct ligation-induced SAP exhibited extensive necrotic areas, inflammatory cells infiltration acinar to ductal metaplasia (ADM) and early fibrosis (Fig. 7A, left). Though free PYD or PTX partially alleviated necrotic areas and ADM, tissue fibrosis and cell death were still present. However, both drugs in nanoparticles showed stronger efficacy in this situation. Significantly reduced lesions of necrosis lesions and acinar cell death indicated that FePTX@CM NPs owned exciting anti-SAP effects. And the lung tissue damage was also weakened after NPs treatment, suggesting less systemic inflammation response was elicited. Also, FePTX@CM NPs gained the best result in the analysis of H&E scores of pancreas (Fig. 7A, right). In the plasma amylase and lipase activity assessment, they were both effectively decreased by FePTX@CM NPs (Fig. 7B). In addition, reduced systemic inflammation also led to decreased plasma levels of IL-1β and IL-6 (Fig. 7C). As shown in Fig. 7D, the result of 16s rRNA in plasma which reflected the bacteria invasion into circulation exhibited an evident reduction in all treatment groups, particularly in FePTX@CM NPs group. TUNEL results showed significant cell death in model group, while much less cell death was present in all treatment groups, particularly in FePTX@CM NPs group (Fig. 7E). The semi-quantitative analysis further confirmed this conclusion. In immunofluorescence staining assay, more macrophages and neutrophils were infiltrated in the pancreas of the control group, while FePTX@CM NPs intervention demonstrated the most effective therapeutic effect in reducing pro-inflammatory cell infiltration (Fig. 7F and 7G).

Accordingly, by establishing two SAP mouse models, we confirmed that FePTX@CM NPs effectively alleviate inflammatory cell infiltration and pro-inflammatory responses, inhibit the release of pancreatic enzymes into the plasma, and protect pancreatic cells from cell death. These results encouraged us to translate the NPs into clinics.

Anti-SAP molecular mechanisms exploration of FePTX@CM NPs in vivo

As mentioned above, the major components of FePTX@CM NPs included PYD and PTX. Our cell-level results demonstrated that PYD inhibited the release of amylase and lipase to prevent self-digestion of the pancreas, while PTX protected macrophages from PANoptosis, thereby limiting the cascade of inflammatory responses. To verify our theories in vivo, FePTX@CM NPs were administered to the caerulein-induced SAP model. The pancreases were harvested and subjected to frozen tissue sectioning for subsequent immunofluorescence (IF) staining. In Fig. 8A-B, we assessed mtROS levels using mitoSOX Green staining and evaluated Golgi stress using GM130 staining. It was evident that FePTX@CM NPs significantly reduced intracellular mtROS levels compared to the

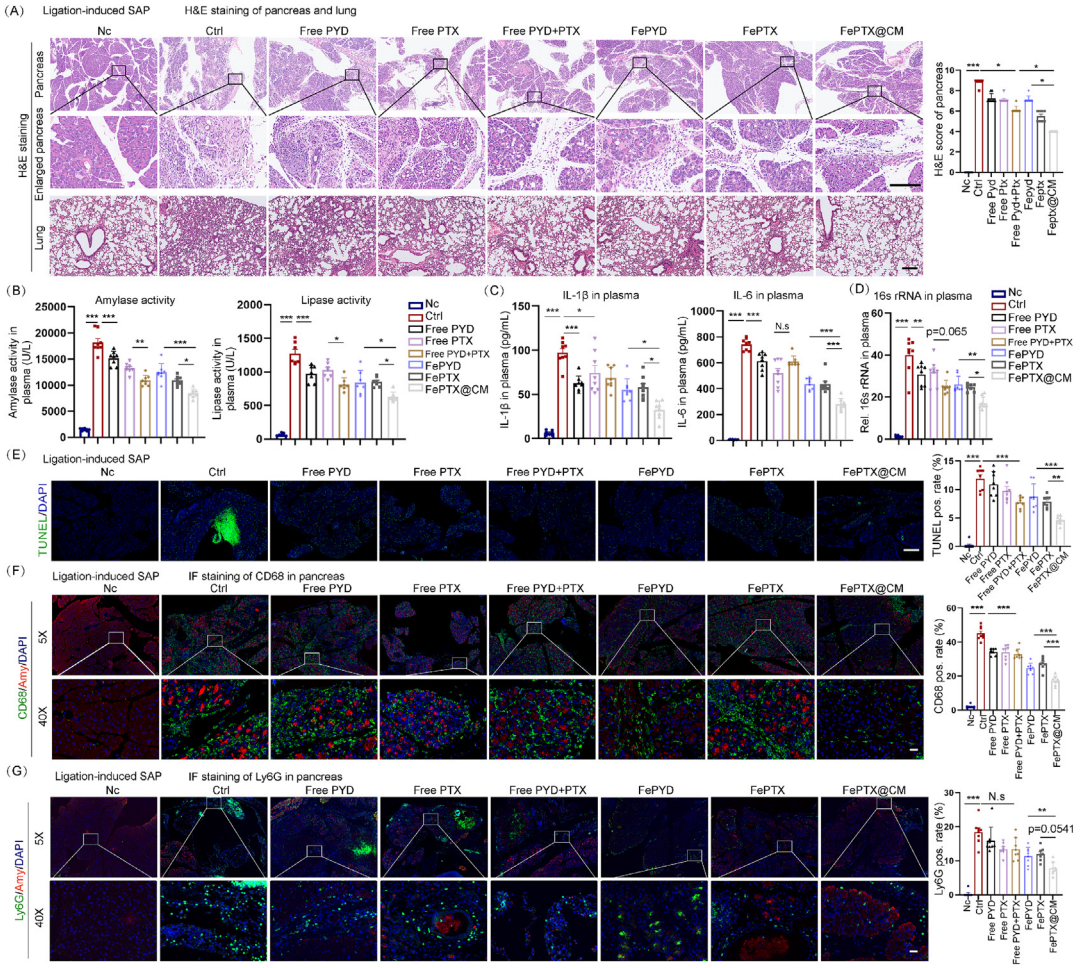

Fig. 7. Efficacy of FePTX@CM against duct ligation-induced SAP model (n = 8). (A) H&E staining images of pancreas and lungs with different interventions and statistical analysis. Scale bar = 200 μm. (B) Amylase and lipase activity in plasma of each group. (C) Plasma level of IL-1β and IL-6 of each group. (D) Result of 16s rRNA in plasma of each group. (E) TUNEL images of each group after treatments. Scale bar = 100 μm. (F-G) Fluorescent images of macrophages and neutrophils in pancreas after various interventions. Scale bar = 25 μm.*P < 0.05, **P < 0.01, ***P < 0.001. N.s. = no significance. Data = mean ± SD.

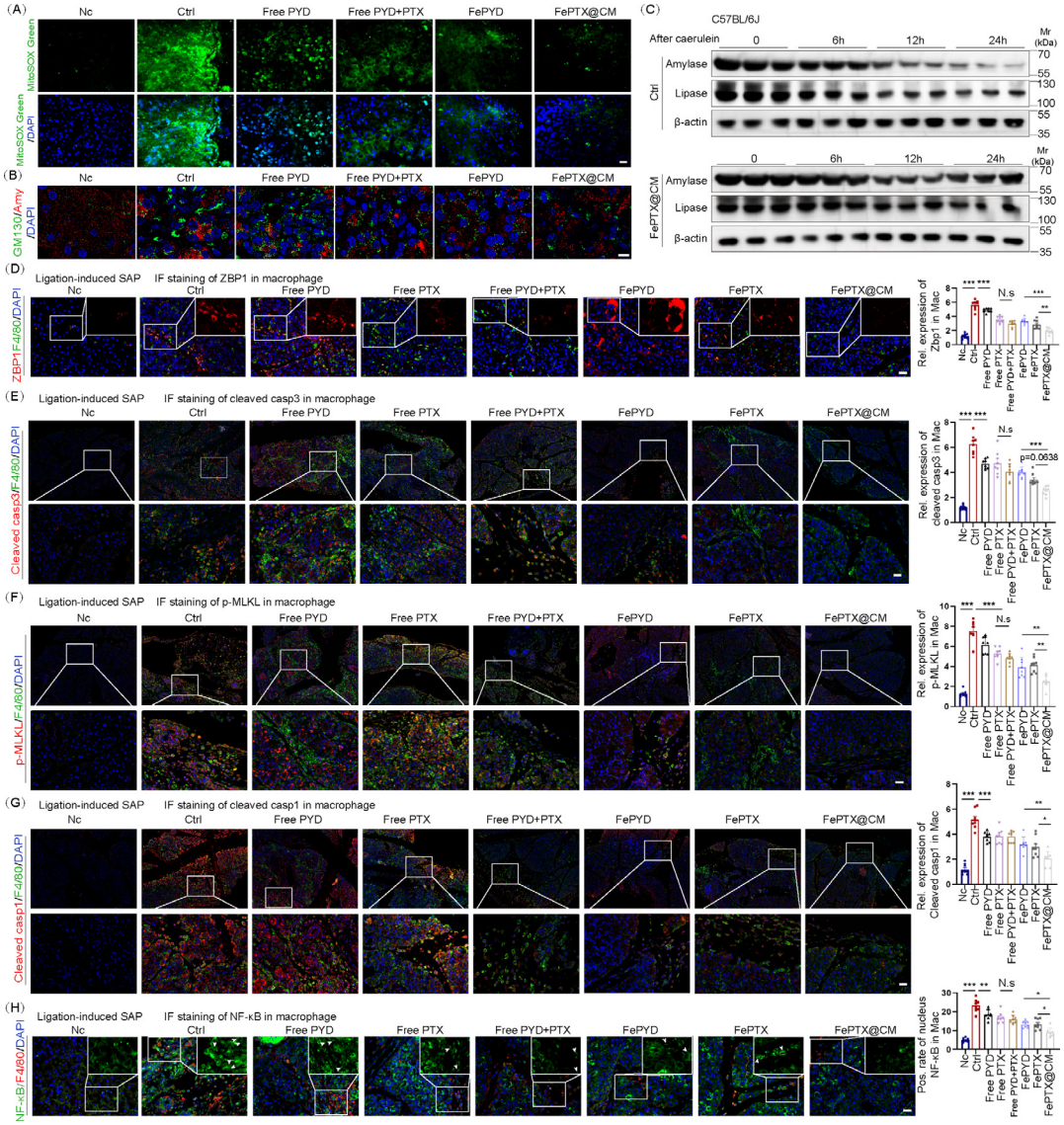

Fig. 8. Mechanisms study of FePTX@CM NPs against SAP in vivo (n = 8). (A-B) Fluorescent images of mtROS and Golgi stress biomarkers in primary pancreas after different treatments and statistical analysis. Scale bar of A = 25 μm, B = 10 μm. (C) Results of western blot for detection of amylase and lipase in pancreas of C57BL/6J after FePTX@CM NPs treatments. (D) IF images of Zbp1 in pancreas in vivo and statistical analysis. Scale bar = 25 μm. (E) IF images of cleaved caspase3 in pancreas in vivo and statistical analysis. Scale bar = 25 μm. (F) IF images of p-MLKL in pancreas in vivo and statistical analysis. Scale bar = 25 μm. (G) IF images of cleaved caspase1 in pancreas in vivo and statistical analysis. Scale bar = 25 μm. (H) IF images of NF-κB in pancreas in vivo and statistical analysis. Scale bar = 25 μm. *P < 0.05, **P < 0.01, ***P < 0.001. N.s. = no significance. Data = mean ± SD.

control group. Additionally, fewer Golgi structures showed damage due to Golgi stress in the FePTX@CM NPs group, as indicated by GM130 staining. Furthermore, pancreas was collected to analyze the preservation of amylase and lipase by western blot assay after treatment of FePTX@CM NPs. As shown in Fig. 8C and Fig. S9, the results demonstrated that caerulein treatment provoked the release of amylase and lipase in a time-dependent manner within 24 h. However, the FePTX@CM NPs-treated acinar cells exhibited higher intracellular levels of these two enzymes, resulting in less harm to the surrounding cells. Thus, our results demonstrated that the inhibition of pancreatic enzyme release mediated by the mtROS/Golgi stress signaling pathway is essential for the anti-SAP effects of FePTX@CM NPs, both in vitro and in vivo.

On the other aspect, in vitro experiments suggested that FePTX@CM NPs could effectively prevent macrophages from undergoing PANoptosis, thereby alleviating the inflammation responses remarkably. To obtain in vivo evidence supporting our observations, we utilized antibodies for PANoptosis-related biomarkers (cleaved caspase 3, cleaved caspase 1, and p-MLKL) and Zbp1 along with F4/80 antibody to label macrophages, allowing us to visualize PANoptosis in macrophages within the SAP model. In Fig. 8D, the expression levels of Zbp1 of macrophage in each group followed a similar trend as observed in the in vitro experiments, further confirming that macrophage PANoptosis was mediated by the Zbp1 signaling pathway, as mentioned above. Meanwhile, the expression of PANoptosis biomarkers (red fluorescence) was also observed to be minimized by FePTX@CM NPs intervention. Simultaneously, mono-application of either free PYD or PTX provided less inhibition against PANoptosis in macrophages. Furthermore, the nucleus location of NF-κB in macrophage was also obviously inhibited by FePTX@CM NPs (Fig. 8H). Therefore, the FePTX@CM NPs treatment demonstrated a remarkable

anti-inflammatory effect on the pancreas by inhibiting macrophage PANoptosis and reducing the release of pro-inflammatory mediators during SAP. Collectively, PYD in FePTX@CM NPs reduced the recruitment of macrophages and neutrophils and alleviated mtROS/Golgi stress-mediated pancreatic enzyme release. Meanwhile, PTX suppressed Zbp1-mediated macrophage PANoptosis, further mitigating the pro-inflammatory response to protect the pancreas in SAP.

In summary, PYD and PTX incorporated in our NPs (FePTX@CM NPs) have the potential to treat SAP both in vitro and in vivo. The mechanisms involved include the inhibition of PANoptosis in macrophages and the suppression of mtROS/Golgi stress-mediated release of pancreatic enzymes in acinar cells. We hope this nano-delivery system offers a novel approach to alleviate SAP in clinical settings and minimizes the impairment of multiple organ functions during the disease process.

Conclusion and prospects

SAP is linked to a high incidence and mortality rate. SAP is characterized by severe tissue cell death, amplified inflammation response and oxidative stress, etc. Early control of the cascade inflammation reactions and acinar cells' function is of great significance to avoid systemic responses. Facing such a dilemma, we prepared a multifunctional FePTX@CM NPs to achieve the purpose of pancreas targeting, inflammation suppression, inhibition of pancreatic enzyme release and prevention of death of acinar cells. The polyphenol, PYD enabled the NPs anti-release of pancreatic enzyme and anti-inflammation ability. We found that the suppression effect of PYD towards pancreatic enzymes (such as amylase and lipase) was achieved by alleviating mtROS/Golgi stress pathway. The newly discovered signal pathway may provide a promising target in drug development. Additionally, it was confirmed that polyphenols could mediate the targeted delivery of polyphenol/antioxidant enzyme complexes to mitochondria. This affinity is not dependent on mitochondrial membrane potential, but rather originates from the strong binding between polyphenol and mitochondrial outer membrane proteins [19]. Therefore, we speculated that our NPs may also reduce mtROS after PYD affiliates with mitochondria. And PTX encapsulated in the NPs exhibited exciting capacity to limit macrophages and neutrophils recruitment, help macrophage avoid PANoptosis via the Zbp1 signal pathway, decrease proinflammatory mediators release, thus relieving inflammation, pancreas injury and lung damage. The excellent efficacy of FePTX@CM NPs against SAP brings surprise to us, nevertheless, there are still some problems that need to be further studied. For example, this study did not explore the synergistic effect of FePTX@CM NPs with current anti-SAP methods. And the prognosis of SAP after FePTX@CM NPs treatment needed further investigation. Collectively, our NPs exhibited good targeting ability, biocompatibility and excellent efficacy, therefore leading to rapid relief of clinical symptoms of SAP. This new combination nanoparticle form of PYD and PTX offers a valuable reference to SAP first aid, and provides a novel approach to develop current drugs with better efficacy and less toxicity.

Ethics approval and consent to participate

Male C57BL/6J (6–8 weeks old) were obtained from SJA Laboratory Animal Co., LTD (Changsha, China) and housed following the guidelines of the Institutional Animal Care and Use Committee (IACUC). Animal experiments were performed according to the protocols approved by the Second Xiangya hospital of Central South University Ethics Committee and abide by the animal care and use guidelines (No. 20230897).

Declaration of competing interest

The authors declare that they have no known competing financial interests or personal relationships that could have appeared to influence the work reported in this paper.

Acknowledgements

This research was supported by National Natural Science Foundation of China (No. 82304424), Natural Science Foundation of Hunan Province (No.2024JJ4081), Changsha Natural Science Foundation (No. kq2208308), Hunan Provincial Health Commission Health Research Project (No. W20243029), Science and Technology Innovation Program of Hunan Province (2024RC3061).

Appendix A. Supplementary data

Supplementary data to this article can be found online at https://doi.org/10.1016/j.jare.2025.04.006.

References

[1] Zerem E, Kurtcehajic A, Kunosić S, Zerem Malkočević D, Zerem O. Current trends in acute pancreatitis: Diagnostic and therapeutic challenges. World J Gastroenterol 2023 May 14;29(18):2747–63.
[2] Wiley MB, Mehrotra K, Bauer J, Yazici C, Bialkowska AB, Jung B. Acute pancreatitis: Current clinical approaches, molecular pathophysiology, and potential therapeutics. Pancreas 2023 Jul 1;52(6). e335–43.
[3] Liu Y, Cui H, Mei C, Cui M, He Q, Wang Q, et al. Sirtuin4 alleviates severe acute pancreatitis by regulating HIF-1α/HO-1 mediated ferroptosis. Cell Death Dis 2023 Oct 21;14(10):694.
[4] He J, Hou X, Wu J, Wang K, Qi X, Wei Z, et al. Hspb1 protects against severe acute pancreatitis by attenuating apoptosis and ferroptosis via interacting with anxa2 to restore the antioxidative activity of prdx1. Int J Biol Sci 2024;20(5):1707–28.
[5] Sohail Z, Shaikh H, Iqbal N, Parkash O. Acute pancreatitis: A narrative review. JPMA J Pak Med Assoc 2024 May;74(5):953–8.
[6] Habtezion A, Gukovskaya AS, Pandol SJ. Acute pancreatitis: A multifaceted set of organelle and cellular interactions. Gastroenterology 2019 May;156(7):1941–50.
[7] Yang H, Cao R, Zhou F, Wang B, Xu Q, Li R, et al. The role of interleukin-22 in severe acute pancreatitis. Mol Med 2024 May;15(30):60.
[8] Sun JK, Lv C, Gao L, Mao W, Li W, Ke L. Nutrition therapy in critically ill patients with severe acute pancreatitis. Nutr Clin Pract Off Publ Am Soc Parenter Enter Nutr 2024 Apr;39(2):271–80.
[9] Tenner S, Vege SS, Sheth SG, Sauer B, Yang A, Conwell DL, et al. American college of gastroenterology guidelines: Management of acute pancreatitis. Am J Gastroenterol 2024 Mar 1;119(3):419–37.
[10] Hamesch K, Hollenbach M, Guilabert L, Lahmer T, Koch A. Practical management of severe acute pancreatitis. Eur J Intern Med 2025 Mar;133:1–13.
[11] Anghel AC, Țăranu I, Orțan A, Marcu Spinu S, Dragoi Cudalbeanu M, Rosu PM, et al. Polyphenols and microbiota modulation: Insights from swine and other animal models for human therapeutic strategies. Mol Basel Switz 2024 Dec 20;29(24):6026.
[12] Su Z, Yao B, Liu G, Fang J. Polyphenols as potential preventers of osteoporosis: A comprehensive review on antioxidant and anti-inflammatory effects, molecular mechanisms, and signal pathways in bone metabolism. J Nutr Biochem 2024 Jan;123:109488.
[13] Wen E, Cao Y, He S, Zhang Y, You L, Wang T, et al. The mitochondria-targeted kaempferol nanoparticle ameliorates severe acute pancreatitis. J Nanobiotechnology 2024 Apr 3;22(1):148.
[14] Niu C, Zhang J, Okolo PI. Therapeutic potential of plant polyphenols in acute pancreatitis. Inflammopharmacology 2025 Feb;33(2):785–98.
[15] Zhao Y, Jiang C, Lu J, Sun Y, Cui Y. Research progress of proanthocyanidins and anthocyanidins. Phytother Res PTR 2023 Jun;37(6):2552–77.
[16] Xu Y, Luo Y, Weng Z, Xu H, Zhang W, Li Q, et al. Microenvironment-responsive metal-phenolic nanozyme release platform with antibacterial, ROS scavenging, and osteogenesis for periodontitis. ACS Nano 2023 Oct 10;17(19):18732–46.
[17] Yuan H, Wang F, Wang Z, Gu D, Huang W, Fu C, et al. Natural metal polyphenol nanozyme: Free radical scavenging and antioxidation for the treatment of acute kidney injury. ACS Mater Lett 2023 Oct 2;5(10):2807–19.
[18] Zhu Y, Huang X, Deng Z, Bai T, Gao B, Xu C, et al. Orally biomimetic metal-phenolic nanozyme with quadruple safeguards for intestinal homeostasis to ameliorate ulcerative colitis. J Nanobiotechnology 2024 Sep 6;22(1):545.
[19] Zhang J, Gao B, Ye B, Sun Z, Qian Z, Yu L, et al. Mitochondrial-targeted delivery of polyphenol-mediated antioxidases complexes against pyroptosis and inflammatory diseases. Adv Mater 2023 Mar;35(11):2208571.

[20] Li J, Zeng H, Li L, Yang Q, He L, Dong M. Advanced generation therapeutics: Biomimetic nanodelivery system for tumor immunotherapy. ACS Nano 2023 Dec 26;17(24):24593–618.
[21] Wang Q, Xu W, Li Q, He C, Liu Y, Liu J, et al. Coaxial electrostatic spray-based preparation of localization missile liposomes on a microfluidic chip for targeted treatment of triple-negative breast cancer. Int J Pharm 2023 Aug;643:123220.
[22] Li YJ, Wu JY, Wang JM, Hu XB, Cai JX, Xiang DX. Gemcitabine loaded autologous exosomes for effective and safe chemotherapy of pancreatic cancer. Acta Biomater 2020 Jan;101:519–30.
[23] Xu WJ, Cai JX, Li YJ, Wu JY, Xiang D. Recent progress of macrophage vesicle-based drug delivery systems. Drug Deliv Transl Res 2022 Oct;12 (10):2287–302.
[24] Li Y, Li H, Zhang K, Xu C, Wang J, Li Z, et al. Genetically engineered membrane-coated nanoparticles for enhanced prostate-specific membrane antigen targeting and ferroptosis treatment of castration-resistant prostate cancer. Adv Sci Weinh Baden-Wurtt Ger 2024 Sep;11(33):e2401095.
[25] Paulis G, Paulis A. Oxidative mechanism of peyronie's disease and effectiveness of pentoxifylline in the therapeutic management: A narrative review. Antioxid Basel Switz 2025 Feb 12;14(2):208.
[26] De Campos T, Deree J, Martins JO, Loomis WH, Shenvi E, Putnam JG, et al. Pentoxifylline attenuates pulmonary inflammation and neutrophil activation in experimental acute pancreatitis. Pancreas 2008 Jul;37(1):42–9.
[27] Fan HN, Chen W, Fan LN, Wu JT, Zhu JS, Zhang J. Macrophages-derived p38α promotes the experimental severe acute pancreatitis by regulating inflammation and autophagy. Int Immunopharmacol 2019 Dec;77: 105940.
[28] Karki R, Lee S, Mall R, Pandian N, Wang Y, Sharma BR, et al. ZBP1-dependent inflammatory cell death, PANoptosis, and cytokine storm disrupt IFN therapeutic efficacy during coronavirus infection. Sci Immunol. 2022 Aug 26;7(74):eabo6294.
[29] Han SL, Abe Y, Miyauchi K, Watanabe Y, Sato N, Kimura S. Therapeutic efficacy of an antineutrophil monoclonal antibody, Urge-8, against acute necrotizing pancreatitis in rats. Surgery 1996 May;119(5):585–91.
[30] Inoue S. Anti-Neutrophil Antibody Attenuates the Severity of Acute Lung Injury in Rats With Experimental Acute Pancreatitis. Arch Surg 1995 Jan 1;130(1):93.
[31] Lee PJ, Papachristou GI. New insights into acute pancreatitis. Nat Rev Gastroenterol Hepatol 2019 Aug;16(8):479–96.
[32] Glaubitz J, Wilden A, Frost F, Ameling S, Homuth G, Mazloum H, et al. Activated regulatory T-cells promote duodenal bacterial translocation into necrotic areas in severe acute pancreatitis. Gut 2023 Jul;72(7):1355–69.
[33] Sendler M, van den Brandt C, Glaubitz J, Wilden A, Golchert J, Weiss FU, et al. NLRP3 inflammasome regulates development of systemic inflammatory response and compensatory anti-inflammatory response syndromes in mice with acute pancreatitis. Gastroenterology 2020 Jan;158(1):253–269.e14.
[34] Zhang C, Li G, Lu T, Liu L, Sui Y, Bai R, et al. The interaction of microbiome and pancreas in acute pancreatitis. Biomolecules 2023 Dec 31;14(1):59.
[35] Kaurani L, Islam MR, Heilbronner U, Krüger DM, Zhou J, Methi A, et al. Regulation of Zbp1 by miR-99b-5p in microglia controls the development of schizophrenia-like symptoms in mice. EMBO J 2024 Apr 16;43(8):1420–44.
[36] Gu W, Pan F, Singer RH. Blocking β-catenin binding to the *ZBP1* promoter represses *ZBP1* expression, leading to increased proliferation and migration of metastatic breast-cancer cells. J Cell Sci 2009 Jun 1;122(11):1895–905.
[37] Li Y, Guo X, Hu C, Du Y, Guo C, Wang Di, et al. Type I IFN operates pyroptosis and necroptosis during multidrug-resistant a. baumannii infection. Cell Death Differ 2018 Jul;25(7):1304–18.
[38] Jakkampudi A, Jangala R, Reddy BR, Mitnala S, Reddy DN, Talukdar R. NF-κB in acute pancreatitis: Mechanisms and therapeutic potential. Pancreatology 2016 Jul;16(4):477–88.
[39] Cen ME, Wang F, Su Y, Zhang WJ, Sun B, Wang G. Gastrointestinal microecology: A crucial and potential target in acute pancreatitis. Apoptosis 2018 Aug;23(7–8):377–87.